CLAS12 Run-group H Experiments with a Transversely Polarized Target

Contents

Abstract

We propose an optimized experimental configuration to meet the goals of three C2 conditionally approved CLAS12 deep-inelastic scattering (DIS) experiments with a transversely polarized target, identified as run-group H. The usage of a transversely polarized Hydrogen target in conjunction with the CLAS12 spectrometer and a 11 GeV polarized electron beam will provide access to unique aspects of the nucleon structure at the scale of confinement. In particular, RGH experiments will measure transverse target single- and double-spin asymmetries in semi-inclusive and hard-exclusive reactions to chase some of the most elusive and peculiar parton distribution and correlation functions among the transverse momentum dependent (TMDs) and generalized (GPDs) families.

C12-11-111 will study the semi-inclusive reaction $ep^{\uparrow} \to ehX$, (with h an identified hadron and X the undetected final state), to access leading-twist parton distribution functions in a transversely polarized nucleon. The transversity, the Sivers function and the so-called "pretzelosity" function describe the correlation between the transverse nucleon polarization and, respectively, the transverse polarization of partons, the transverse momentum of unpolarized partons and the transverse momentum of transversely polarized partons. Furthermore, double-spin asymmetries based on both the target transverse and the beam longitudinal polarizations will provide access to the so-called "worm-gear" function, sensitive to the correlation between the transverse momentum of longitudinally polarized partons and the nucleon transverse polarization. RGH data will also provide constraints to the transverse-momentum dependent Collins fragmentation function.

C12-12-009 will study the semi-inclusive reaction $ep^{\uparrow} \to eh_1h_2X$ (with h_1 and h_2 two identified final state hadrons) to access the transversity distribution and its first moment, the tensor charge, in a reaction that can be described by a standard collinear formalism and provides a benchmark for the alternate transverse-momentum dependent (TMD) extraction.

C12-12-010 will measure the deeply-virtual Compton scattering (DVCS) $ep^{\uparrow} \to ep\gamma$, whose azimuthal asymmetries depend on different combinations of GPDs, to provide access to the elusive GPD-E sensitive to the contributions of u and d flavors to the total quark orbital angular momentum. Double-spin asymmetries will be measured simultaneously, giving access to the real part of the target spin dependent DVCS amplitude.

This set of experiments will contribute to a comprehensive investigation of the nucleon structure in the CEBAF energy domain performed with the same spectrometer. The x, Q^2, z, P_{hT} dependencies will be studied in a wide kinematic range thanks to the large acceptance of CLAS12. Flavor sensitivity will be ensured by the available excellent particle identification systems. In order to disentangle the relevant kinematic regimes, in particular related to the perturbative (in P_{hT}) and twist (in Q) leading contributions, a total of 110 days of beam time is requested for these experiment.

1 Executive Summary

The CLAS12 run-group H (RGH) comprises 3 experiments with a transversely polarized target originally approved with rating A by PAC39 [1] and selected among the high-impact JLab measurements by PAC42 [2]:

- **C12-11-111** *Transverse spin effects in SIDIS at 11 GeV with a transversely polarized target using CLAS12*: a multi-dimensional analysis of the semi-inclusive deep-inelastic scattering (SIDIS) reactions to access transversity and tensor charge, and the Sivers and Collins functions connected with the spin-orbit phenomena of the strong-force dynamics [3];
- **C12-12-009** *Measurement of transversity with dihadron production in SIDIS with transversely polarized target*: a multi-dimensional analysis of the SIDIS reactions at 11 GeV exploiting the dynamics of the dihadron final state to access transversity in the benchmark collinear limit and investigate novel parton correlations inaccessible on the single hadron case [4];
- **C12-12-010** *Deeply Virtual Compton Scattering at 11 GeV with transversely polarized target using the CLAS12 Detector*: a multi-dimensional analysis of the DVCS reaction to access the most elusive Generalized Parton Distribution entering the orbital momentum sum rule (Ji sum rule) [5].

All the three experiments got a C1 condition to address the technical issues related to the target performance. During the jeopardy process at PAC52, their status changed with a C2 condition to assess in more details the revised experimental configuration, in particular regarding the achievable physics impact in conjunction with the required beam-time [6].

The RGH experiments pursue a science case of utmost interest as highlighted in the current 2023 NSAC Long Range Plan. They anticipated sensitivity on several crucial observables whose knowledge is severely limited by the sparse data available. The RGH experiments are a precursor and complementary to one of the pillars of the EIC science programs [7, 8] and will to cover the valence phase space with unprecedented precision. Distinctive features in common of all the three RGH experiments are the precise measurement of parton distributions and phenomena in an unexplored valence region where current models project their magnitude to be peaking, a luminosity at least one order of magnitude higher than the previous experiments, a large acceptance detector for the disentanglement of the various correlations and kinematic regimes, an excellent particle identification capability to access flavor sensitivity.

The adopted solution foreseen a dynamically polarized NH_3 target with a dedicated recoil detector replacing the CLAS12 solenoid and Central Detector. Such a solution favors consolidated technologies and builds up from previous successful realizations at JLab. The achievable luminosity is defined by the background level in the experiment and the nominal $\mathcal{L} = 5 \times 10^{33}$ cm^{-2}s^{-1} RGH value corresponds to the most realistic (real-data) and conservative (present CLAS12 capability without ongoing upgrades) estimate and requires a modest beam current of few nA. To be competitive with lattice calculations on the u-flavor tensor charge and supersede the available GPD $\mathrm{E_u}$ information, a total of 110 PAC days are requested (10 PAC days of commissioning and calibration).

2 Physics Motivation

In the recent years, new parton distributions (PDFs) and fragmentation functions (FFs) have been introduced to describe the rich complexity of the hadron structure, focusing on the parton transverse degrees of freedom at the scale of confinement and moving toward the achievement of a 3D description of the parton dynamics. Relevant examples are transverse momentum dependent (TMD) and generalized (GPD) parton distributions, relating the longitudinal momentum fraction (referred to the direction of the hard probe) with the intrinsic partonic transverse momentum or position, respectively. Their detailed investigation requires a novel level of sophistication in the deep-inelastic scattering (DIS) experiments that should conjugate precision, in discriminating semi-inclusive and exclusive reaction details, and power, in collecting large amount of data to allow multi-dimensional analyses.

The CLAS12 run-group H program collects several fundamental measurements that provide access to elusive quantities and are only possible with the use of a transversely polarized target in conjunction with a large acceptance high-precision spectrometer.

The **Transversity** PDF describes the parton transverse polarization inside a transversely polarized nucleon, reflects the relativistic nature of the parton confinement and exhibits peculiar evolution properties. It is the least well known leading PDF that does not vanish when integrated in the parton transverse momentum $k_\perp$, and can thus be studied in the collinear limit. Although essential for the nucleon description, due to its chirally-odd nature transversity has only recently been accessed in a limited kinematic range and with a large uncertainty that still prevents a reliable flavor decomposition [9]. Its first moment in Bjorken x, the tensor charge, is a fundamental quantity in quantum chromodynamics (QCD) connected to searches of beyond Standard Model phenomena such as the Electric Dipole Moment (EDM) of particles [10] and the tensor interaction [11]. CLAS12 data will cover an unexplored kinematic regime at high Bjorken-x. As the integral of transversity, the tensor-charge is dominated by the contribution at high-x in the valence quark region. While this is true for many polarization dependent PDFs, this feature is even stronger for transversity as the contribution from gluons is vanishing due to its chiral-odd nature. Recent phenomenological extractions [12] peak in the region of $x > 0.3$ where world data is very sparse. The missing data might explain the current tensions between extractions from data and the lattice. Therefore the proposed run group will provide needed constraints to the tensor charge and allowing precise comparison with lattice QCD, which has made remarkable progresses in the past decades [13].

The **Sivers** PDF is a genuine TMD function which vanishes with $k_\perp$ integration. Among the most intriguing parton distributions, it requires a non-zero parton orbital angular momentum and a correlation with the nucleon spin. As a consequence of its non-trivial gauge-invariant definition, the Sivers function probes QCD at the amplitude level: it is naively T-odd (do not violate T-invariance due to the interaction phase) and exhibits a peculiar process dependence. A sign change is expected when moving from SIDIS to Drell-Yan processes, whose verification is one of the most urgent goals of the present experimental activity [9]. It is among the few TMDs that, while describing the non-perturbative nature when $k_\perp \ll Q^2$, should in principle match the perturbative regime with increasing transverse momentum, providing a formal bridge between the two QCD descriptions [14]. CLAS12 data will allow an extended coverage in the valence region and a disentaglement of the Sivers kinematic dependences, a crucial information for the study of these phenomena and the connections among different QCD regimes.

The **Collins** and **Di-hadron** FFs originate from spin-orbit effects connecting the spin of a fragmenting quark with the final observed hadron or dihadron transverse momentum, respectively. Convincing evidences have been found for the existence of these mechanisms [9]. These peculiar FFs act as a quark polarimeter and allow to access the elusive chirally-odd distribution functions in SIDIS reactions. In particular the Di-hdaron FF, sensitive to the hadron pair *relative* transverse momentum, can be studied in the collinear limit providing a complementary access to transversity that does not depend on the TMD formalism, and can be reliably extended to the hadron-hadron scattering case [15]. High precision data from CLAS12 can complement present and future information gathered at the much higher center-of-mass energy of experiments at the e^+e^- colliders [16], like BELLE-II, and at hadron-hadron colliders, like PHENIX and STAR [17].

The **GPD E** describes asymmetries in the parton spatial distribution that imprint the underlying confinement dynamics. It it the least know GPD that enters the Ji sum rule [18] quantifying the parton orbital momentum [19]. Its measurement in the golden deeply-virtual Compton scattering (DVCS) channel requires the usage of a transversely polarized target in case of protons, or the measurement of a beam-spin asymmetry off an unpolarized target in case of neutrons [20]. As the latter is among the goals of RGB experiments that already took data, both measurements can be accomplished at CLAS12 providing an unprecedented level of information.

It is worth mentioning that, besides the selected fundamental measurements discussed above, many other important observables can be measured simultaneously with a transversely polarized target. In practice, in fact, azimuthal amplitudes sensitive to the poorly known leading-twist "pretzelosity" $h_{1T}^\perp$ and "worm-gear" g_{1T} TMDs, as well as to several sub-leadings-twist transverse-momentum-dependent PDFs and FFs [21, 9] can be extracted simultaneously in the analysis of the same data. Furthermore, the poorly known transversity (chiral-odd) GPDs H_T and $\tilde{H}_T$ can be accessed in deeply virtual pseudo-scalar meson production (DVMP) with a transversely polarized target [22, 23].

Since the last jeopardy review in 2020, few new results became available on the electro-production of mesons off a transversely polarized target. COMPASS published the study on dihadron transverse-spin-dependent asymmetry on proton and deuterium targets [24], and the results on the deuteron data from 2022 run [25]. HERMES completed a multi-dimensional fit [26] and COMPASS a P_T-weighted analysis [27] of already published data. All these results are limited to Bjorken x below 0.3. COMPASS published preliminary Drell-Yan data consistent with the fundamental QCD prediction of a sign change of naive time-reversal-odd TMD PDFs (i.e. Sivers) when comparing the Drell-Yan process with SIDIS [28]. The interest in data on transversely polarized targets is manifest from the continue flow of phenomenological analyses of the sparse SIDIS data collected in the past couple of decades, in conjunction with proton-proton, e^+e^- and Drell-Yan data [29, 30]. The SoLID experiment [31, 32] has been mentioned as strategic opportunity in the 2023 Long Range Plan for Nuclear Science and is awaiting CD0. No new DVCS results on transversely polarized targets became available after HERMES [33, 34] and RGH experiments provides the first chance to overcome the lack of information. New channels of investigation are being explored [35, 36] and phenomenological study is awaiting new inputs [37, 38]. Lattice calculations are making steadily progresses [39, 40] and can offer benchmark quantities or complementary constraints to the phenomenological models.

3 Experimental Details

The experiment exploits the CEBAF high quality beam [41] in conjunction with the large acceptance CLAS12 spectrometer [42] in Hall-B, complemented with a transversely polarized target (see Sec. 4.1) and a dedicated recoil detector (see Sec. 4.3).

3.1 CLAS12 Spectrometer

The CLAS12 spectrometer has been designed to run at high luminosity, up to about 3 orders of magnitude larger than the precursor experiments like HERMES and COMPASS, and bring the 3D nucleon structure study into the precision phase. CLAS12 started the data-taking with unpolarized hydrogen targets in spring 2018 and has been running successfully so far with different targets and detector configurations. In particular, CLAS12 successfully ran with longitudinally polarized NH_3 and ND_3 targets in 2022-2023. Detailed calibration procedures and event reconstruction algorithms have been developed to reach a performance close to, or in same case superior of, the design specifications.

3.1.1 Forward Detector

With respect the goals of run-group H, the spectrometer has specifically demonstrated to be able to achieve the following performance.

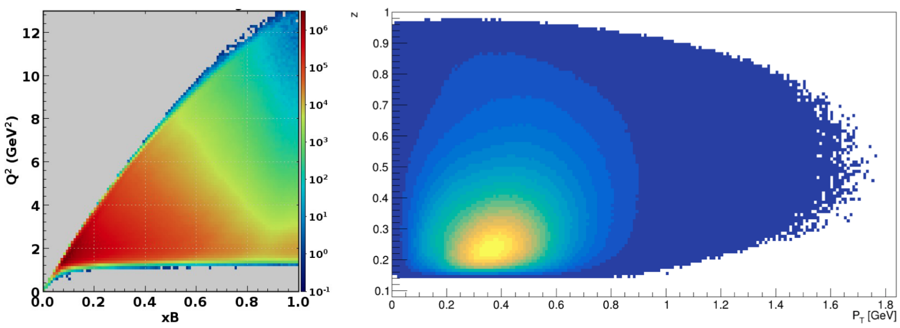

Fig. 1: (Left) The CLAS12 reach in the relevant kinematic variables at a beam energy of 10.6 GeV. (Left) Inclusive electron coverage in the hard scale Q^2 versus Bjorken x. (Right) Charged hadrons coverage in the transverse momentum P_T versus the fractional energy z.

Tracking The single-track forward reconstruction efficiency has been improved with the implementation of ML algorithm to support effective denoising and track segment finding, to a level of better than 90% at the design luminosity of 1×10^{35} cm^{-2}s^{-1}, with a dependence on the beam current of $98 - 0.1 \times \mathrm{I}\,(\mathrm{nA})$ percent. The typical measured resolutions in the relevant kinematic quantities are $\Delta p/p = 0.67\%$, $\Delta\theta = 0.85$ mrad and $\Delta v_z = 4.6$ mm, in line with the design specifications of a resolution better than 1% in momentum and 1 mrad in polar angle [42].

Scattering Electron The efficiency of the CLAS12 trigger for DIS events, with the electron scattered inside the acceptance at an energy above 1.5 GeV, is greater than 99% [43]. Electrons are identified by a combination of signals in the Cherenkov counters and calorimeters. Thanks to the large acceptance of CLAS12, scattered electrons are detected in a wide kinematic range from elastic events to DIS with an extended reach at large values of Q^2, Bjorken x, and forward hadron kinematics, see Fig. 1.

Exclusive events Events selection and background suppression has been successfully achieved in the CLAS12 environment. The large amount and variety of collected data and the gained experience provide a solid ground for any new development. For example, a study is ongoing to exploit machine-learning techniques for the identification of exclusive DVCS events based on the electron and photon information provided by the CLAS12 Forward Detector but no (or partial) recoil information. Promising results have been obtained on RGA data, with increased statistics and comparable physics observable with respect the traditional analysis based on a complete recoil reconstruction.

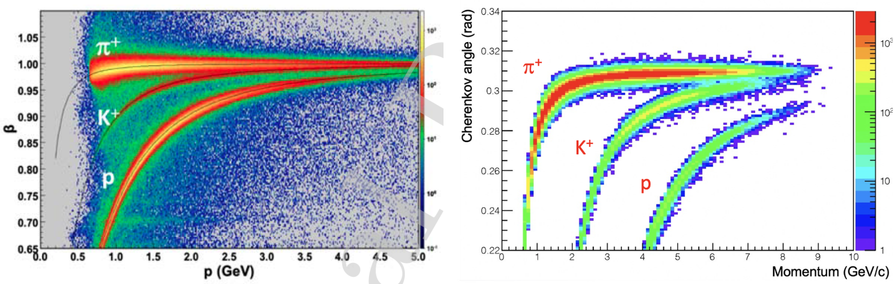

Fig. 2: (Left) The hadron separation provided by the Forward time-of-flight system. (Right) The hadron separation obtained by the RICH detector.

Hadron PID Identification of hadron particles is essential to gather flavor information in SIDIS observables. The CLAS12 forward time-of-flight system (FTOF) provides an excellent pion separation from kaons and protons at momenta up to about 3 GeV/c and 5 GeV/c [44], respectively, see left panel of Fig. 2. To complement such CLAS12 baseline configuration and provide hadron separation in the whole range of interest for SIDIS physics, up to momenta of 8 GeV/c, a ring-imaging Cherenkov detector (RICH) has been anticipated at the time of the proposal. The RICH has been designed as composed by two modules in a left-right symmetric configuration, to reduce the systematic effects in observables dependent on the target transverse polarization. The peculiar geometry of CLAS12 suggested an innovative hybrid-optics solution to limit the active area to about 1 m^2 per sector, with part of the light directly imaged and part of the light detected after reflection from mirrors. In order to limit the material inside the acceptance and realize a light but stiff structure, composite materials derived from aeronautic applications have been employed. Improvements have been pursued in all the components, achieving the world leading aerogel radiator clarity of 0.0050 $\mu\text{m}^4\,\text{cm}^{-1}$ at high refractive index (n=1.05), a 20% reduction of the aereal density of spherical mirrors in carbon fiber composite polymer with respect the LHCb realization, the first use of glass-skin planar mirrors in a nuclear physics experiment, the first use of the flat-panel multianode H12700 photomultiplier with a dynode structure dedicated to the single photon detection. As part of the RGH preparation, the first module was installed in 2018 before the start of CLAS12 data taking and the RICH completed in 2022 before the start of the RGC polarized target run [45]. Ongoing data analysis shows that the CLAS12 RICH is able to match the required time and Cherenkov angle resolutions, and provide hadron separation in the wanted momentum range, see right panel of Fig. 2.

3.2 Beam Elements

The standard beam-line equipment in Hall-B comprise position, current and halo monitors connected to the interlock system. Among the Beam Position Monitors (BPMs), three nA BPMs, (2C21 at the beginning of the tunnel, 2C24 at the end of the tunnel before the hall proper, and 2H01 on the space frame), measure beam transfer (x,y) position relative to their center as well as the beam current. The stripline BPMs (2H00 close to the target and other on the upstream tunnel) measures beam position but are reliable only for beam currents above 25 nA and will not be used by RGH. The position monitor 2H01 (together with 2H00 if the current is high enough) close to the interaction region is the most important one to keep the beam position steady on the target. A feedback system (the orbit locks) uses (x,y) positions on this BPM, and the Horizontal and Vertical correctors on 2C22/2C23/2H00 girders to keep the beam position stable.

The Hall-B Faraday cup provides an instantaneous beam current reading. It is not cooled and cannot operate at high currents but works fine at 1 nA, with an integrated rate of 906.2 counts/sec. The Synchrotron Light Monitor (SLM) measures amount of synchrotron light generated by electron beam in the magnetic field of the last dipole right before the Hall-B upstream tunnel. The main use of this current monitor is to measure helicity related beam intensity (charge) asymmetry but can be used for beam charge accounting if needed.

The beam halo counters consist of photomultiplier tubes with plastic attached to their photocathodes strapped to the beam pipes along the beamline. The rates in halo counters are good indicators of the beam transport quality. In addition to the halo counters, there is a beam offset monitor (BOM) just upstream of the target.

The CLAS12 beam line has already operated at a beam current of 1 nA. Some specific monitor can not work at this low beam current, but there is enough redundancy in current and position monitors to ensure a normal operation and safe control. The same beam raster utilized for the RG-C operations will be used (note the target material is the same), with a radius envelope of 6.5 mm and a frequency of 1 Hz.

4 Required Equipment

4.1 Transverse Target

The experiments described here will utilize a new, dynamically polarized target of solid ammonia (NH_3) specifically designed to operate inside the HTCC. The ammonia samples will be continuously polarized using microwave-induced spin flip transitions at a temperature of 1 K and in a 5 T magnetic field. Similar target systems have been used with success at JLab in experimental halls A, B, and C [46, 47, 48] and with electron beam currents up to 140 nA. Most recently, a longitudinally polarized target of NH_3 and ND_3 was used for the Run Group C experiments with CLAS12 [49]. In this system, the 5 T polarizing field was provided by the CLAS12 solenoid, which will be removed for Run Group H in order to install a 5 T split-coil magnet with a vertical field orientation. While the magnetic field requirements for frozen spin polarized targets are less stringent, beam heating and radiation damage exclude their use in the CEBAF electron beam [50].

The target considered here will resemble a compact version of the system used in Hall C and Hall A and most recently described Pierce *et al.* [46]. A vertical ladder suspends multiple target cells into a pumped bath of superfluid helium at 1 K (Fig. 3). For the RGH experiments, the ladder will have two cells ($\varnothing 1.5 \times 2.0$) cm^3 filled with 1–2 mm granules of frozen ammonia, an empty cell, as well as carbon and polyethylene (CH_2) samples for background and dilution studies. As has been the case in the Hall A and C polarized targets, small NMR coils will be inserted into the ammonia cells for measuring the proton polarization with a relative accuracy of about 4%. The cells are fabricated from PCTFE, a fluorinated plastic that is transparent to the 140 GHz microwaves for polarizing the ammonia but does not produce a background proton NMR signal. Thin aluminum windows are glued to the upstream and downstream faces of the cell. The superfluid bath is constrained by a thin-walled aluminum tube. The superfluid and aluminum windows contribute to the overall scattering at the level of about 20%.

Liquid helium to the target will be supplied by the Hall B buffer dewar and pumped to a vapor pressure of approximately 0.1 torr by a set of high-capacity Roots pumps. Each target cell will contain about 2 g of solid ammonia and will require less than 0.5 W of microwave power for optimum polarization. Heat from the 1 nA beam will deposit less than 10 mW.

The 5 T superconducting magnet will be similar in design to the split-coil magnet intended for transversely polarized target experiments in Hall C. Unfortunately, this magnet was designed for a horizontal field orientation and cannot provide the 60° aperture for scattered protons that is needed for the DVCS portion of this proposal. The superconducting windings of the new magnet will be identical to the existing magnet but will be separated by an aluminum frame with a more favorable geometry for RGH. The magnet and 1 K refrigerator will be housed in a vacuum chamber with a thin aluminum exit window matching the aperture of the 5 T magnet.

Based on previous experience at JLab, proton polarizations of 90% or higher can be expected. Radiation damage from the electron beam slowly destroys the polarization, and so the beam will be rastered over the face the target to reduce this effect. After a dose of about 2.5×10^{15} e^{-1}cm^{-2}, the damage can be

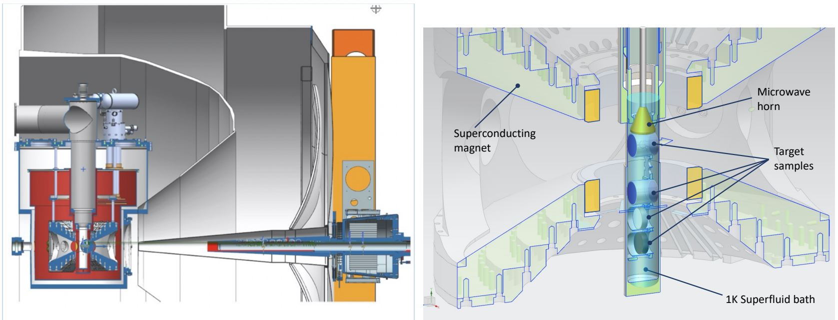

Fig. 3: Left: Conceptual design showing the dynamically polarized target at the center of the CLAS12 HTCC. Right: Closeup of target samples suspended in superfluid helium.

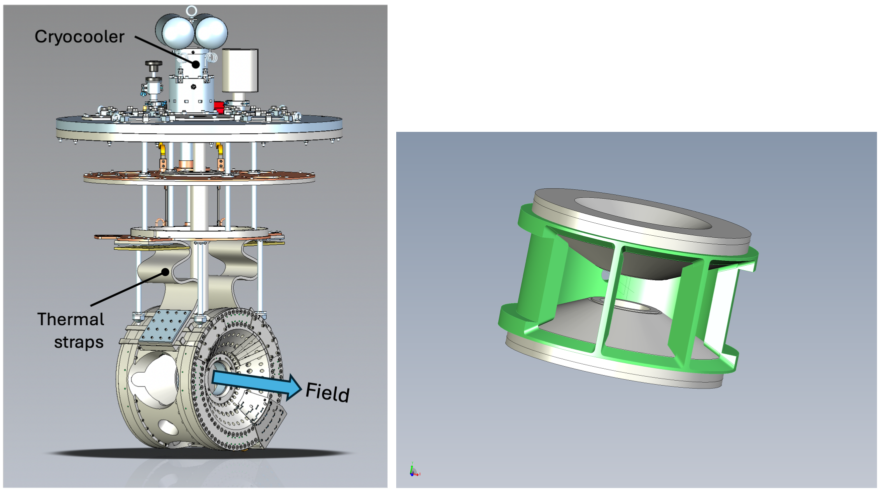

Fig. 4: Left: Superconducting magnet for polarized target experiments in Hall C. The magnet has been successfully tested to 5 T at Jefferson Lab. Right: Conceptual redesign of the magnet coils with a different intercoil support (green) for RGH. The opening in the forward directions for scattered particles spans ±60° in the horizontal plane and ±25° in the vertical. The magnet is rotated to produce a vertical field.

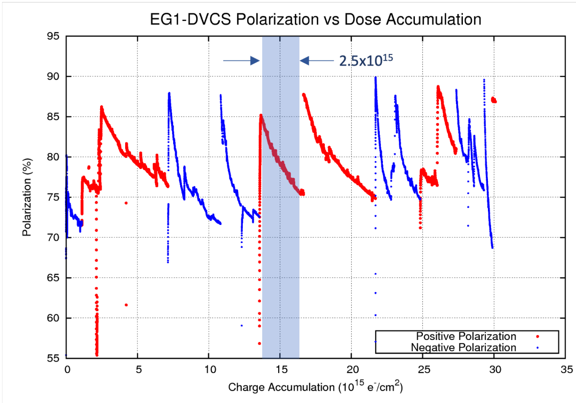

Fig. 5: Performance of the 6 GeV CLAS polarized target during the EG1-DVCS experiment. The shaded band indicates a depolarizing dose of 2.5×10^{15} $e^{-1}cm^{-2}$.

partially repaired by annealing the sample to about 90 K for several minutes (Fig. 5). Assuming a beam current of 1 nA and a raster diameter of 7 cm, an ammonia sample can last approximately six days before annealing is necessary. However, the annealing procedure, which can be performed *in situ*, becomes progressively less successful, and the ammonia must be replaced after about five or six anneals. With two ammonia samples on the ladder, this corresponds to about 80 days of beam on target.

4.2 Beam Chicane

The 5 T polarizing field of the target is transverse to the beam. Its integral of XX Tm implies a deflection of 2.1 degrees for 10.6 GeV beam particles. A magnet chicane has been designed in order to compensate such a bending and ensure that the non-interacting particles pass by the experiment, and reach the Hall-B dump within the vacuum pipe of the experiment, without further interactions.

The chicane need to be compact to fit within the constrained space of the Hall-B beam line. A workable solution has been outlined that is compatible with the other beam element and the CLAS12 solenoid, when the latter is moved into a park position, see Figure 6. It can be realized with commercially available superconducting split-pair magnets, see Figure 7. With respect to items in stock, minor modifications are required: change orientation of the cooling head and enalarging the bore of the exit window of the cryostat. The field uniformity is sufficient to avoid beam orbit perturbations even accounting for a rastered beam with a radius envelope of 7 mm, see Section 3.2.

The beam chicane generates synchrotron radiation upstream of the detector. According to analytic estimates and past experience, no real issue was anticipated. Nevertheless a dedicated study has been pursued with GEANT simulation. The chicane model has been implemented in the GEMC framework used by CLAS12, see Figure 8. The field of the chicane magnets has been rescaled by 0.89 to match the same field integral of the target magnet. The central magnets have been moved off axis by 11 cm to align with the bended

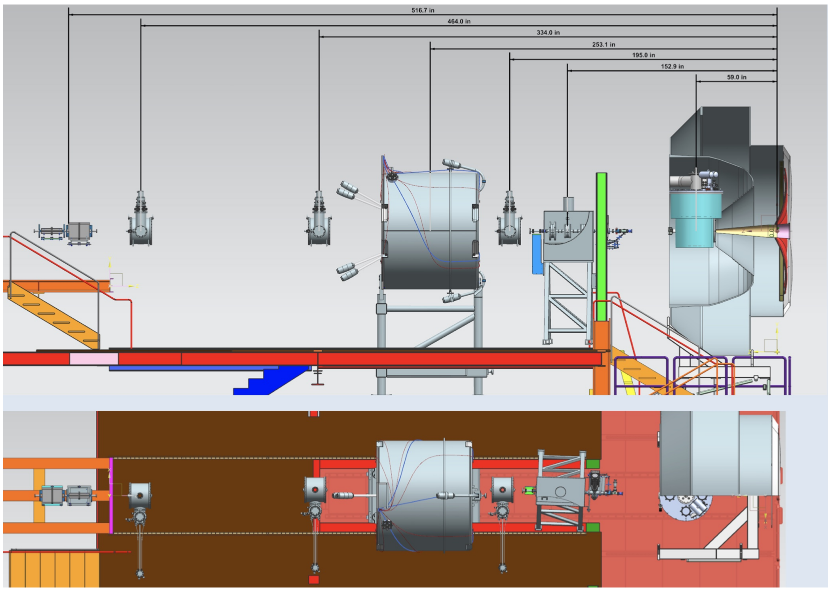

Fig. 6: (Left) The magnet chicane to compensate the beam bending of the target holding magnet (left). The 7.5 T split-pair magnet from CryoMagnets inc. (right).

beam. Simulations show that the beam stays centered through the chicane, impinges on the target at the wanted angle and is aligned downstream to the axis of the CLAS12 vacuum pipe, see Figure 9. The photons are generated in the bending sections of the line (where a significant magnetic field is present) and span an horizontal flare that could extend into CLAS12 in absence of any material. The beam pipe itself, plus 15 mm lead shield in the relevant positions, are enough to effectively suppress these photons. The vast majority of the synchroton radiation generated close to the interaction region is trapped inside the downstream CLAS12 vacuum pipe. The 1% surviving fraction escapes the vacuum pipe due to rescattering. This amounts to an O(1 GHz) photon flux distributed over the etire multi squared-meter surface of the CLAS12 Forward Detector, see Figure 10. Simulations show that this flux does not generate any significant background in the experiment, as expected by its low energy spectrum peaked at 0.1 MeV.

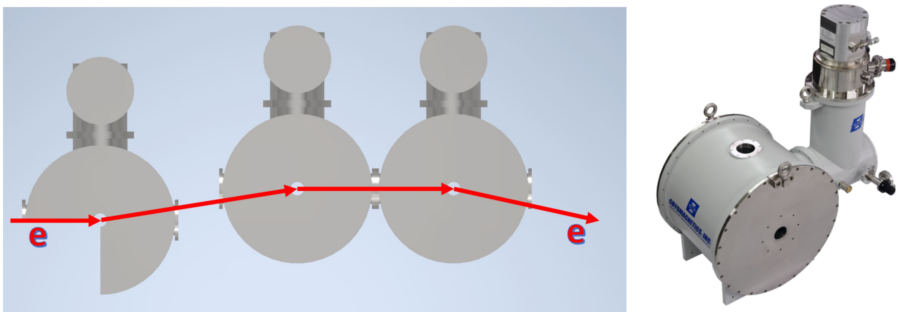

Fig. 7: (Left) The magnet chicane to compensate the beam bending of the target holding magnet (left). The 7.5 T split-pair magnet from CryoMagnets inc. (right).

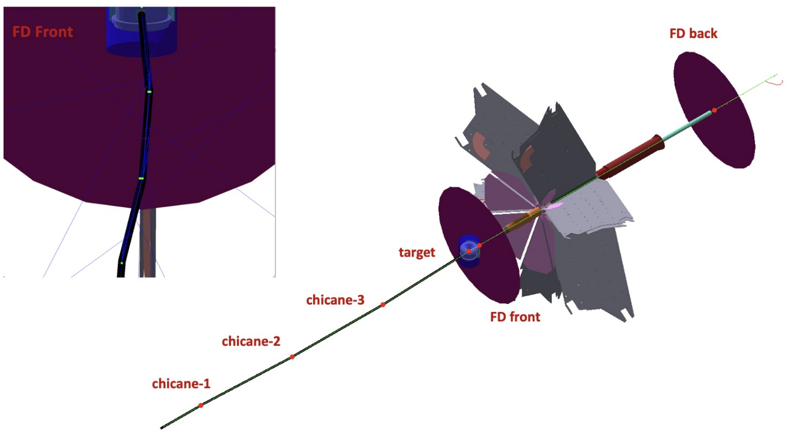

Fig. 8: The magnet chicane implemented in the CLAS12 GEMC simulation framework. The passing particle are recorded by flux planes at the magnet locations, and on the front and back face of the CLAS12 Forward Detector (only the torus magnet structure is visible for simplicity). The insert shows a section of the beam pipe, with the synchroton photon trajectories shown in blue.

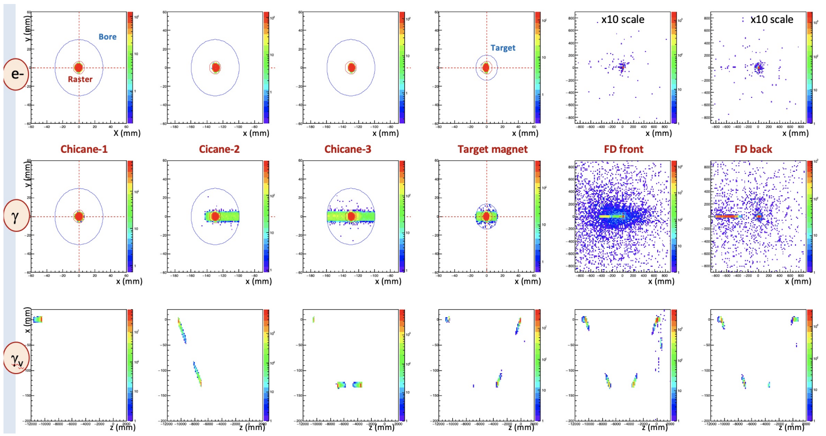

Fig. 9: Spatial distribution of the beam particles on relevant locations along the CLAS12 beam line. From left to right: center of the first, second and third chicane magnet, center of the target magnet, front and back face of the CLAS12 Forward Detector. The electron beam particles are always centered (top row). The photons create a horizontal flare (middle row) because emitted by electrons in the bending sections of the line (bottom row). The beam pipe and shielding have been removed to allow free flight of particles.

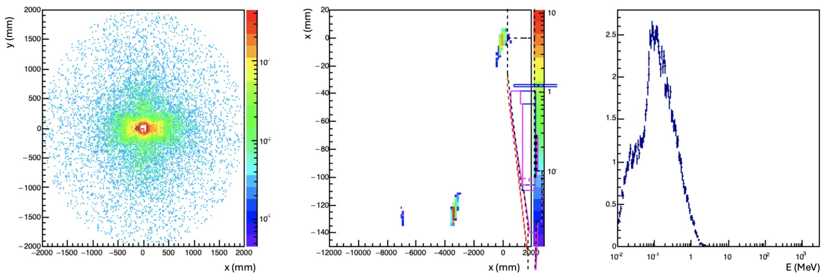

Fig. 10: Spatial distribution at the front of the CLAS12 Forward Detector (left), emission vertex position (center) and energy spectrum (right) of the synchrotron photons escaping the beam pipe and a 15 mm lead shielding.

4.3 Recoil Detector

The chosen target magnet structure provides open acceptance in the angular region favored for recoil detection, up to 70 degrees (and beyond, thanks to the magnet bending). Protons below 30 degrees are anyway detected in the CLAS12 Forward Detector. In order to detect protons at larger angles, a dedicated recoil detector can be implemented exploiting the left and right openings in the magnet structure. In each side, a simple geometry based on four detection planes, three tracking and one time-of-flight (TOF) plane, is anticipated. The solid angle coverage should match the magnet apertures and span $\pm$ 25 degrees vertically and 34 degrees horizontally. The distance from IP is chosen to optimize the leverage within the clearance of the CLAS12 HTCC detector, see Table 1.

Plane	Name	Distance from IP (mm)	Width (mm)	Height (mm)
1	Front tracker	340	190	420
2	Mid tracker	550	310	500
3	Back tracker	800	450	560
4	Time-of-flight	1120	630	800

Tab. 1: Basic dimensions of the RGH recoil detector planes covering the magnet apertures on the left and right side of the target.

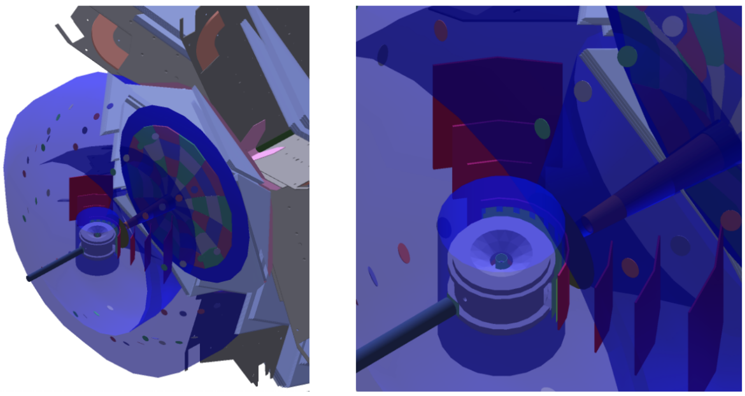

Fig. 11: Concept of the RGH recoil detector in front of CLAS12 HTCC detector.

Simulations indicate that for such a geometry a space resolution of 100 μm for the tracking planes and a time resolution of 100 ns for the TOF plane allow to achieve performance, in angle and momentum reconstruction, that are comparable to the existing Central Detector of CLAS12, see Sec. 4.3.3.

Such a detector does not pose a specific technological challenge. It can be derived from developments with comparable spatial and time resolution already ongoing for the CLAS12 upgrade in luminosity, and for the ePIC detector at EIC. The area to cover is limited, resulting in a manageable number of readout channels, of the order of 10k for tracking and 1k for TOF, see Sec. 4.3.3. The development effort and construction costs can be minimized by borrowing part of the readout electronics.

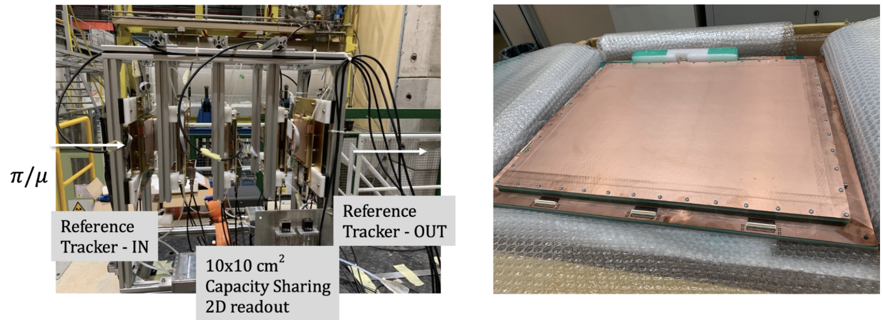

Fig. 12: Set-up used for testing the μRwell performance during a test-beam at the SPS North Area H8C at CERN in June 2023 (left). Large area 40×46 cm^2 μRwell prototype with a 2D cathode readout.

The tracking detector can be derived from the ongoing CLAS12 high-luminosity and ePIC tracking projects based on the μRwell technology, see Sec. 4.3.1. Several 10×10 cm^2 prototypes have been produced at INFN with 2D reading layout of ≈ 0.5 mm strip pitch, approaching a spatial resolution close to 100 μm and a time resolution better than 10 ns, see Fig. 12 (left). The maximum width of the current μRwell foils is 620 mm and therefore compatible with the RGH dimensions. A large area 40×46 cm^2 prototype with a 2D capacity sharing readout has already been realized and is now under test, see Fig. 12 (right). The readout can be largely borrowed from the readout of the GEM chambers produced at INFN for SBS in Hall-A, that are currently stored as spares but will become available after the SBS run. This readout is based on the chip APV25, the same chip in use for the ongoing μRwell prototype tests. As a backup solution, the same readout under study for the high-lumi project and based on the VMM3 chip can be adopted.

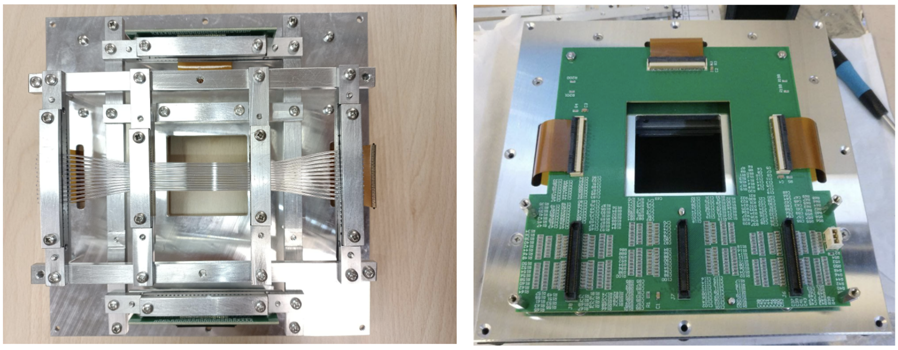

Fig. 13: The scintillating fiber tracking prototype under construction.

To improve the time resolution to a sub-ns level, a plane of scintillating bars readout by SiPMs can be used. Scintillating technology is already well in use at CLAS12 for the forward and central time-of-flight systems (FTOF and CTOF) and the Central Neutron Detector (CND). The SiPM sensors offer a compact and cost-effective solution, that is insensitive to the magnetic fringe fields. Resolutions better than 100 ps have been obtained with fast scintillating rods of few mm thickness, 10 mm width, and variable length [51, 52]. Prototypes based on fibers and rods are being realized at INFN, see e.g. Fig. 13 (left). The readout can be derived (and largely borrowed) from the one of the CLAS12 RICH detector based on the MAROC3 chip, see Fig. 13 (right). This readout has been already successfully used with SiPM matrices for detecting signals down to few photon-electrons, achieving a single-photon time resolution of 0.5 ns largely driven by the FPGA settings. A new firmware is available to push the time resolution to better than 100 ps, provided that a proper clock distribution is implemented as achieved by the ALERT readout. As alternative, a minimum front-end electronics can be designed to match the ADC/TDC readout modules of the CLAS12 timing detectors that are not in use during RGH (CND, CTOF), although this may limit the total channel number.

4.3.1 μRwell Tracking

The modern photolitographic technology on flexible and standard PCB supports has allowed the invention of novel and robust micro-pattern gas detectors (MPGDs), such as GEM [53], THGEM [54, 55] and Micromegas [56]. These detectors exhibit good spatial and time resolution, high rate capability, large sensitive area, flexible geometry, good operational stability and radiation hardness. However, due to the fine structure and the typical micrometric distance of their electrodes, MPGDs generally suffer from spark occurrence that can eventually damage the detector. The micro-Resistive WELL (μRwell) is a compact, simple and robust MPGD developed for large area applications requiring the operation in harsh environment [57]. The detector amplification stage, similar to a GEM foil, is realized with a polyimide structure micro-patterned with a blind-hole matrix, embedded through a thin Diamond-Like-Carbon (DLC) resistive layer with the readout circuit board (PCB). The introduction of a resistive layer mitigates the transition from streamer to spark and gives the possibility to achieve large gains ($> 10^4$) in the presence of high particle rates (up to 10 MHz/cm^2) [58].

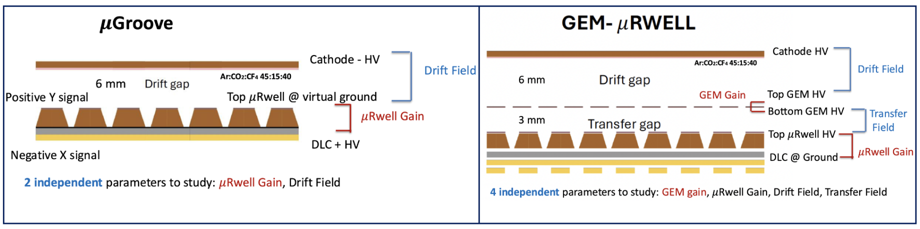

Fig. 14: Alternative architecture under test for obtaining a 2D readout within the same μRwell chamber: Split cathode with a micro-groove plate (left) and GEM-μRwell COMPASS-like stack (right).

The μRwell technology aims to provide micro-pattern gas detectors with performance similar to GEMs but more robust architecture against sparks thanks to the resistive cathode layer. It was originally developed at INFN and is currently under study for the high-luminosity upgrade of CLAS12 and for the inner tracking of ePIC at EIC. The ongoing R&D at INFN has goals that are consistent with the RGH requirements. These are time resolution better than 10 ns, space resolution better than 150 μm, efficiency greater than 95%, low material budget (of the order of 1% χ_0). Different solution are being studied to obtain an optimized 2D (x, y) strip readout within the same chamber with a discrete pitch dimension (of the order of 0.5 mm to contain the number of channels) and sufficient gain. Prototypes have been realized to test the realistic performance in lab and with beam tests. Prototypes of $10 \times 10\,\mathrm{cm}^2$ have been tested in pairs to compare the relative performance. Large prototype of $40 \times 46\,\mathrm{cm}^2$ area, comparable with the RGH needs, have also being successfully produced. Among the tested options, there is a capacitive sharing readout, a top-segmented readout with a segmentation of just the copper layer of the multiplication stage, or the μGroove readout with a fully grooved multiplication stage, see Fig. 14 (left). They typically meet the specifications only at voltages above 600 V, when the chamber became unstable. Promising results have been obtained with a GEM-μRwell COMPASS-like readout, see Fig. 14 (right). In the latter case a gain of $5 \cdot 10^4$ and an efficiency of 97% has been reached at safe voltages around 550 V. The efficiency was measured to be pretty uniform over the detector surface.

The μRwell readout has been studied with the reference APV25 chip that has been a standard for several years [59]. The APV25 is a 128-channel analogue pipeline chip that provides signal sampling with a typical time bin of 25 ns. The basic time information is provided by the sample with the maximum signal amplitude. In order to improve the time resolution, an analysis of the signal shape out of all the recorded samples is required. In this case, a time resolution comparable or better the 5 ns can be obtained. In the basic charge centroid method, the centroid of the cathode signals is used to estimate the position of the impinging particle. It is typically accurate only for trajectories close to 90 degrees with respect to the tracking plane. The μTPC method attempts a more sophisticated analysis to infer the particle angle from the distribution in time and space of the distributed anode signals. It requires adequate time and space resolutions to properly correlate the information. This was demonstrated with the GEM-μRwell prototypes readout by APV25 at the CERN test-beam, see Fig. 15.

The RGH baseline solution is an architecture based on the well-known APV25 chip and derived from the existing GEM tracker development for Hall-A SBS. The front-end APV card mounting the chip features 128 analog channels, 40 MHz (25 ns) signal sampling, up to 130 analog sample pipeline per channel, 3.4 μs trigger latency, and 100 kHz rate multiplexed readout, see Fig. 16. Up to 16 APV cards (2048 channels) can be connected via HDMI cables to a single MPD VME board. The MPD mounts a Arriga GX FPGA with 128 MB DDR2-RAM and provides FIR filter, common mode and pedestal subtraction, zero suppression, remote configuration, and 2 ns trigger resolution, see Fig. 17. Up to 32 MPDs can be connected to a single SSP module via optical fiber links. The SSP module has been developed by the JLab fast-electronics group and is already in use at CLAS12 (i.e. for the RICH readout).

The SBS readout electronics and firmware have been developed by INFN in

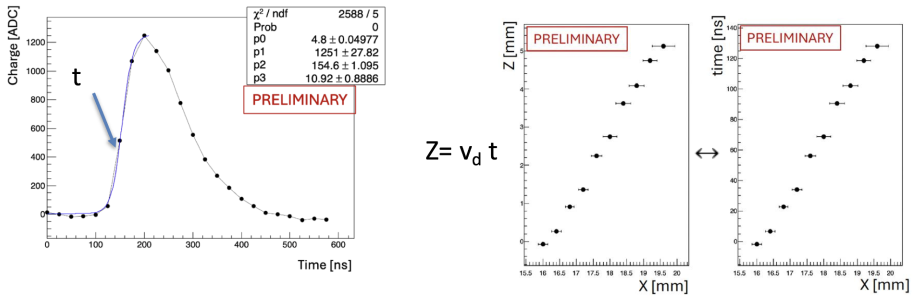

Fig. 15: Example of fit of the μRwell sampled signal to maximize the time resolution (left) and correlation in time and space obtained with the μTPC method (right).

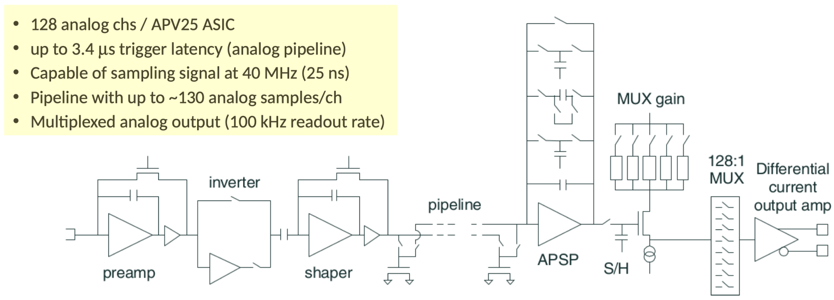

Fig. 16: The APV25 chip logic diagram and main features.

collaboration with JLab. INFN has available at JLab more than 270 APV cards (35000 channels) and 24 MPD boards that can be re-allocated with the end of the SBS run. INFN has also available one VME/VSX crate and a SSP module. The main INFN groups and expertise involved in the SBS tracker readout, i.e. INFN-RM1 with Evaristo Cisbani and INFN-GE with Paolo Musico, are part of the RGH recoil project and can support its development. One example is the work in progress to develop a new version of the MPD module. Beyond an upgrade to more modern and powerful FPGAs, the new module aims to move from VME to 1GB/s Ethernet connection, support a trigger rate up to 30 KHz with an increase number of samples, and provide new cabling options to APV25.

The VMM3 chip foreseen for the CLAS12 high-lumi upgrade can offer a backup solution for the readout. INFN personnel at INFN-GE involved in the development of a readout chain based in this chip is part of RGH.

The SBS front-tracker has an expected rate up to 500 kHz/cm^2 and an estimated strip occupancy of 60%. With 3 samples per event and a trigger rate of 5 kHz, the MPD-SSP chain has to be able to cope with a 100 Mb/s transfer rate. To this end no more than 15 APV cards have been connected to the same MPD. The RGH specifications are less stringent. At the foreseen $5\cdot10^{33}$ cm^{-2}s^{-1} luminosity, the expected rate in the RGH recoil detector planes approaches a value close to 300 kHz/cm^2 only in the sheet-of-flame region along

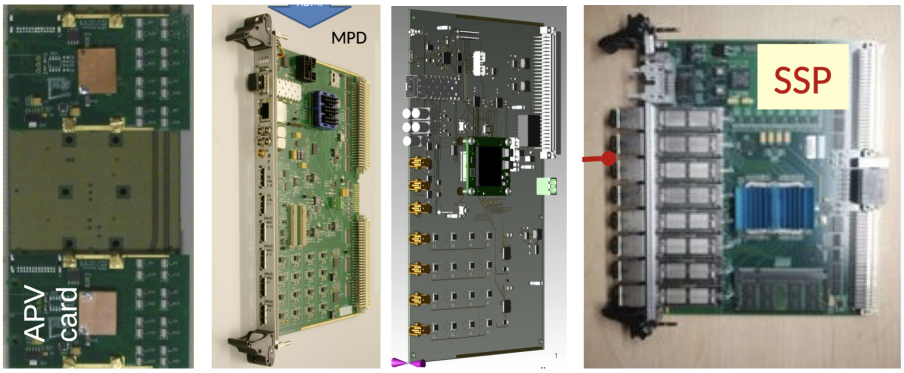

Fig. 17: The essential elements of the SBS tracker APV25 readout chain: the APV front-end card (left), the MPD FPGA board in the existing version and in the upgraded version under development (center) and the SSP data-acquisition module (right).

the bending plane of the magnet, see Fig. 18 and Sec. 4.3.4. In the rest of the detector, the rate is one order of magnitude lower.

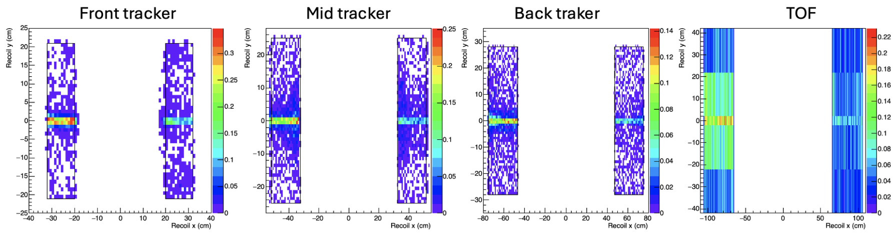

Fig. 18: Expected background rate on the RGH recoil detection planes expressed in MHz/cm^2 for tracking (first three panels) and MHz/ch for TOF (last panel).

4.3.2 Scintillation Timing

The main driven requirements for the RGH recoil timing detector are, in addition to a O(100 ps) time resolution, a compact layout to fit into the HTCC envelope while maximizing the acceptance, and a flexible tessellation to provide matching with μRwell tracks and control of the background accidentals.

The baseline solution is a plane of scintillating bars readout by SiPM sensors. This technology is well known thanks to the studies connected with Medical Imaging [60], and does not require innovative developments to achieve the wanted time resolution once coupled to the right readout electronics [61].

Contained scintillator dimensions naturally mitigate the dependence of the time resolution on the bar geometry and particle impact point. The scintillation light yield is driven by the bar thickness, but the usable light fraction is ultimately dictated by the active area coverage of the bar rim. Being compact, SiPM does not require large thicknesses. Time resolutions better than 100 ps was reported with bars of 5 mm thickness and variable length up to 20 cm [51] and more recently even with bars of 3 mm thickness and 30 cm length [52]. In case of need, more than one SiPM can be connected in series to cover a large rim area while containing the number of readout channels.

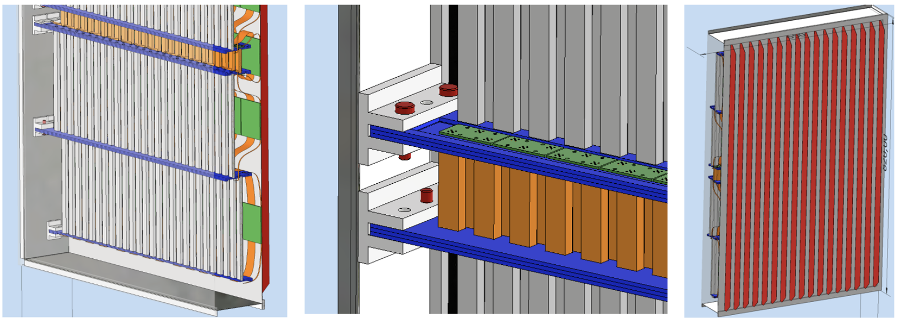

Fig. 19: Concept ot RGH TOF. The timing wall is composed by arrays of vertical scintillating bars readout by SiPMs with the front-end electronics mounted on the downstream support structure (left). Detail of the frame fixing the bars and mounting the sensors (center). The support structure provides cooling and services (right).

Because just a coarse space information is required to match the recoil track, the bar dimensions can be chosen to mitigate the rate of background accidentals. The current design assumes vertical bars with a width of 12 mm and two lengths: 40 mm across the bending plane where background concentrates, and 200 mm outside it. In this way the accidental rate is limited to be below 200 kHz per readout channel, see Fig. 18. The recoil TOF concept is depicted in Fig. 19. The scintillating bars are staggered into arrays and readout on both ends by SiPMs. The bars are vertical to provide best space segmentation in the target magnet bending plane. The timing wall is composed by five arrays of bars whose height is optimized to cope with the background level. The readout electronics is mounted on the downstream supporting structure that provides heat dissipation and services. The front window is minimized in material budget but conductive to provide a Faraday cage. The bars are staggered in order to avoid any dead area due to wrapping or in the region close to the readout electronics.

The readout of the RGH timing SiPMs can be adopted from existing realizations at CLAS12. The easiest solution is to use the spare RICH electronics based on the MAROC3 chip, that is designed for small signals and has been successfully coupled to SiPM in the R&D phase. This chip was successfully run for years at CLAS12, for a Cherenkov application that requires single-photon sensitivity. In the RICH readout, the discriminated signals are fed into a FPGA with implemented a digital TDC with a time bin of 1 ns. A better time resolution was not required for RICH but can be improved with an existing firmware upgrade (developed for ALERT, see below). However the clock distribution architecture, based on optical fiber links and the SSP module, would limit the resolution to something around 100 ps, with a contribution comparable to the sensor.

A better solution is the re-use of the ALERT board design done at JLab and based on the PETIROC chip. PETIROC2 has 32 analog input channels that are independently managed and a dynamic range more suited to a multi-photon regime than MAROC. Each channel is divided into two signals, one for time stamping using a TDC and one for charge measurement. The time branch of each channel is preamplified before it is fed into the TDC developed using a leading edge in addition to a Time-to-Amplitude converter. Time bin is 25 ps resulting in a resolution better than 40 ps, with a latency greater than 10 μs. The charge of the pulse is obtained storing the shaped signal values at its peaking time using a switch capacitor array (SCA). To peaking time is defined with respect a delayed trigger signal produced by the time branch. The ALERT board, see Fig. 20, mounts two PETIROC chips and drives 48 channel SiPM inputs with in individual bias ≈1V trimming. It mounts the same FPGA utilized in the CLAS12 RICH readout with an upgraded TDC firmware of 16 ps bin ensuring an intrinsic time resolution better then 35 ps. In the low noise time over threshold readout mode, it can record a measure proportional to the input charge. The low noise amplification and discrimination chain allow low thresholds (≈ 40 fC) well matched to the expected signal. The clock distribution is done via an ethernet link that preserve a global readout time resolution of about 50 ps, adding a marginal contribution to the one of the sensor.

The development of the ToF detector is synergistic with the R&D activities for a KLM like detector at the EIC [62] and pursued by the group at Duke. This detector would also use scintillator bars with direct SiPM readout optimized for timing resolutions better than 100 ps. Currently, simulations for this detector are well advanced and being adapted for RGH. Similarly, a front end board holding the SiPMs and its amplifier circuit developed within KLM can serve as a benchmark and backup solution for the RGH recoil. Planned cosmic ray test stands for the KLM can also be used for the development of the proposed TOF detector.

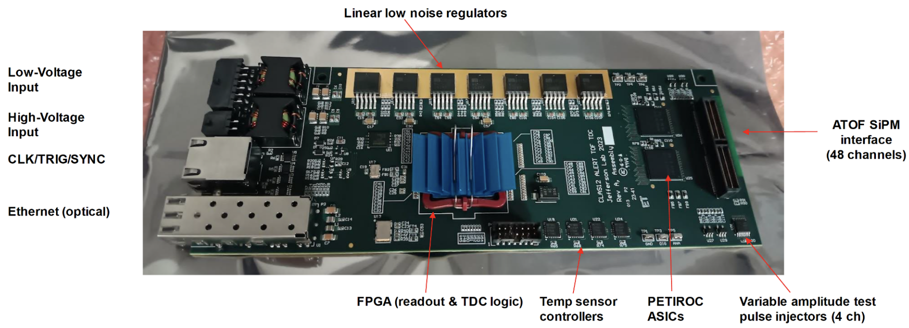

Fig. 20: The ALERT readout board designed by the fast-electronics group at JLab.

4.3.3 Recoil Reconstruction

A preliminary performance study of a RGH recoil as the one detector described above has been performed within the GEMC simulation package based on GEANT. The well developed model of the CLAS12 spectrometer has been complemented with a realistic model of the target and its cryostat that was adapted from previous realizations. The target magnet structure and its holding field have been derived from the Hall-C existing magnet. A simplified description of the RGH recoil detector has been implemented using the flux detector model that records any physics particle passage. This allows an accurate assessment of the acceptance. Spatial coordinates and time information have been smeared according to the wanted resolutions (100 μm and 100 ps, respectively).

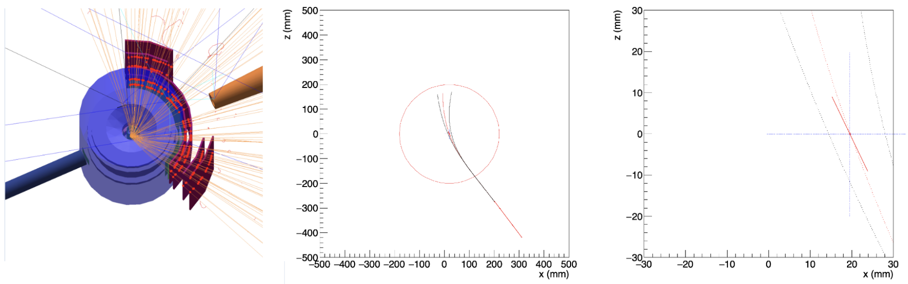

Fig. 21: Typical bending of recoil protons inside the target magnetic field at 0.5 GeV/c (left). Example of the recoil trajectory swimming towards the IP as a function of the assumed momentum (center) and matching to the interaction vertex as defined by the forward electron (right).

The target magnet is designed to concentrate a 5T field in the target volume, but features a modest return field outside the target cryostat. In the tracking section of the RGH recoil, bending is as a consequence limited and here neglected. Rather, the particle momentum is estimated swimming back the recoil trajectory through the known field and requiring a match with the interaction vertex defined by the scattered electron as detected in the CLAS12 forward detector (FD), see Fig. 21. The anticipated resolution of the reference vertex is 5 mm along the beam and 1 mm transverse to it. The first value corresponds to the CLAS12 FD measured performance. The second derives from the precision of the beam rastering system. The vertex matching resembles a kinematical fitting procedure and provide optimized combined resolutions.

Within the above specifications, the obtained performance is comparable to the existing CLAS12 Central Detector, see Fig. 22. The worse resolution in the polar angle σ_θ is not a reason of concern, as the DVCS event reconstruction quality is anyway dominated by the photon measurement in the CLAS12 FD.

A complete RGH recoil model is now been implemented in the CLAS12 simulation package. The layout and digitization details are derived from the indications provided by the ongoing R&D activity, that is synergistic with CLAS12 high-lumi and EIC KLM. Tracking planes are μRwell chambers with 2D readout and 0.5 mm strip pitch to achieve a 100 μm space resolution. TOF planes consists of vertical scintillator rods with 10 mm width and 5 mm thickness to achieve a 100 ps time resolution. To contain accidentals hits and some basic spatial correlation, the rods are organized in 5 rows of two lengths (40 mm in the bending plane, and 200 mm outside). Each rod is readout by two 3×3 mm^2 SiPMs attached at the center of opposite rims. The rods are staggered in order to preserve acceptance over the sensor location, see Fig. 19. This geometry results in the number of channels outlined in Tab. 3.

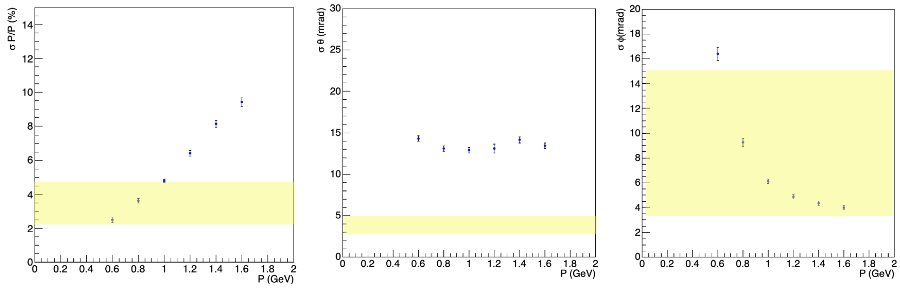

Fig. 22: Simulated resolution on momentum (left), polar angle (center) and azimuthal angle (right) of the RGH recol detector, compared to the typical values of CLAS12 Central Detector (yellow bands).

Plane	Name	x Strip (mm)	y Strip (mm)	Channel N.
1	Front tracker	0.5	0.5	2440
2	Mid tracker	0.5	0.5	3240
3	Back tracker	0.5	0.5	4040
4	Time-of-flight	10	40 and 200	1260

Tab. 2: Granularity and number of readout channels of the RGH recoil detector planes.

4.3.4 Physics Background

A detailed study of the background sources has been performed using a standardized 252 ns acquisition window around the triggered event, indicating three main components. The first component comes from beam particles loosing energy in the target material and bended outside the beam orbit into the detector acceptance, see Fig. 23. They are concentrated in the bending plane of the target magnet and illuminate only one side of the recoil detector, because negatively charged. In most of the cases the background particle transverse all the recoil projective layers and therefore provide 4 space hits (three from tracking and one from TOF). The second background component comes from shower particles generated in the target region, see Fig. 24. These are almost symmetric in charge and therefore illuminate both sides of the detector, but are still concentrated in the bending plane of the target magnet. More than one background particle could be generated in the event, with a recorded hit number which is typically a multiple of 4 (the recoil detector layers). The third background component comes from secondary interactions in the material downstream the target, especially in the shielding material surrounding the CLAS12 beam pipe, Fig. 25. These low-energy particles have an erratic path with an associated casual number of hits in the whole surface of the recoil detection planes.

Preliminary studies indicate that the TOF plane can provide clean seeds for μRwell tracking thanks to its spatial tessellation and time precision. As a consequence, the recoil trajectory can be properly reconstructed in the presence of the background described above.

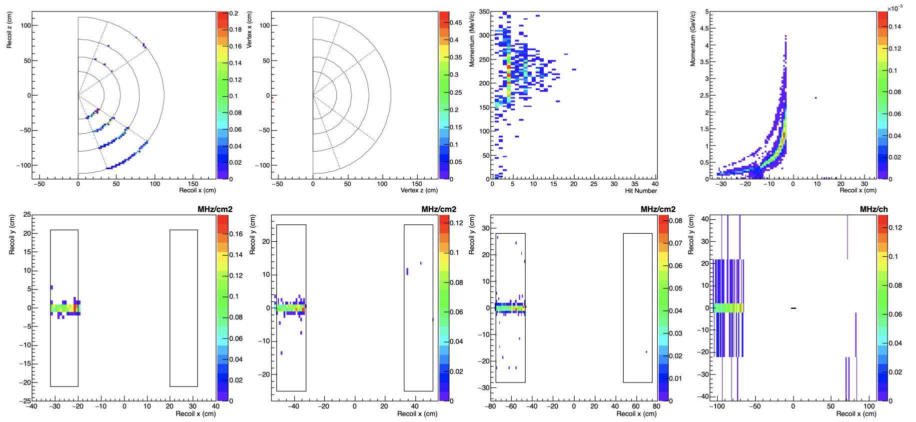

Fig. 23: Expected background on the RGH recoil detection planes (three tracking plus one TOF plane) from beam particles loosing energy into the target material. The top row shows the projection on the bending plane of the recoded hits (left), the location of the originating vertex (center-left), the distribution in momentum and hit multiplicity per particle (center-right) and the correlation between momentum and detected x position on the bending plane (right). The vertex is not visible as far upstream along the beam line. The bottom row shows the background rate (in MHz/cm^{-2} for tracking and MHz/ch for TOF) for the fourth detector layers.

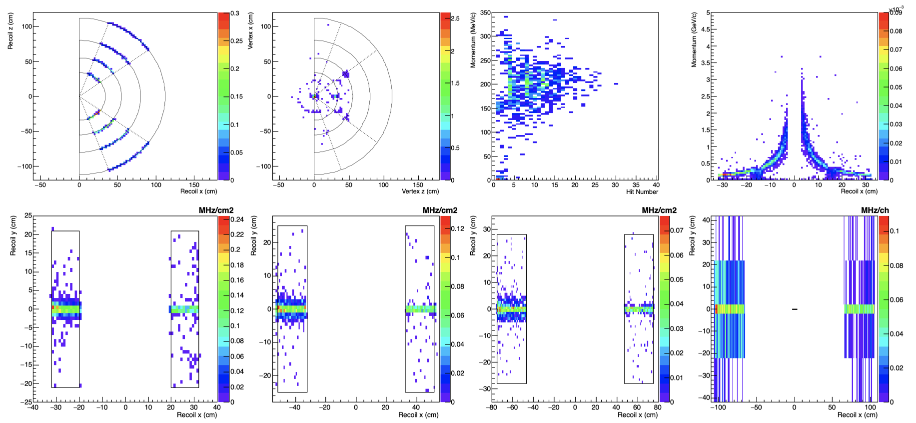

Fig. 24: Expected background on the RGH recoil detection planes (three tracking plus one TOF plane) from shower particle generated into the target material. Panels are organized as in Fig.16.

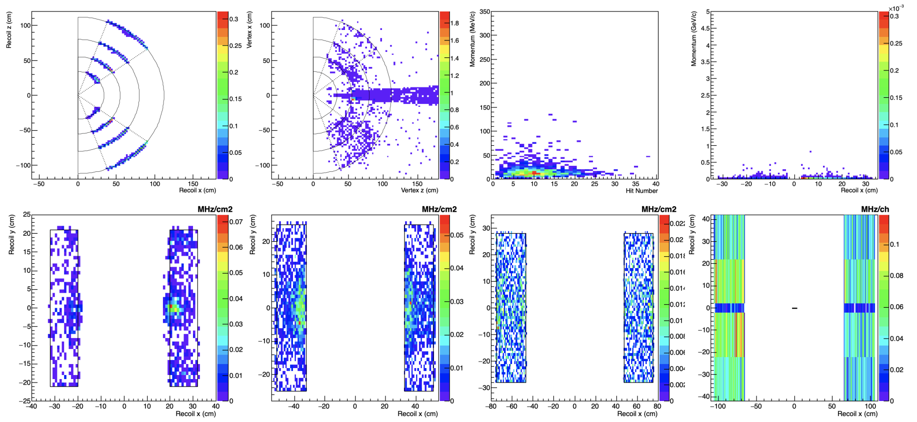

Fig. 25: Expected background on the RGH recoil detection planes (three tracking plus one TOF plane) from secondary interactions downstream the target. Panels are organized as in Fig.16.

4.3.5 Mechanical model

The cryostat of the RGH target and holding magnet is an adaptation of previous realizations in Hall-A and Hall-C. It should fit into the clearance of the HTCC detector together with the newly designed recoil detector, see Figure 26. The RGH target position is assumed to stay the same as the current CLAS12 solenoid center. The cryostat allows for the exchange of the target and annealing of the irradiated targets in situ. It mounts thin aluminum windows for the beam and scattered particles to minimize secondary interactions, see Figure 27. The rectangular exit window is similar to the one realized for the Hydrongen target in Hall-C.

The RGH recoil detector instruments the region of polar angles between 40 and 70 degrees, see Figure 28. This is the angle interval most populated by recoil protons from DVCS reactions, see Figure 29. The support of the recoil detector will be independent from the one of the target cryostat to allow target maintenance or substitution without impact on the alignment, see Figure 30.

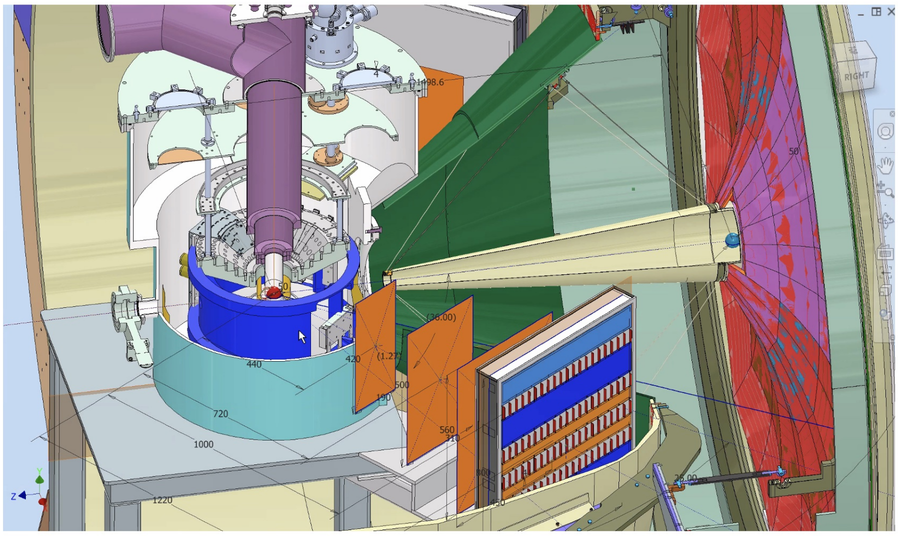

Fig. 26: Overview of the RGH target and recoil system inside the HTCC clearance.

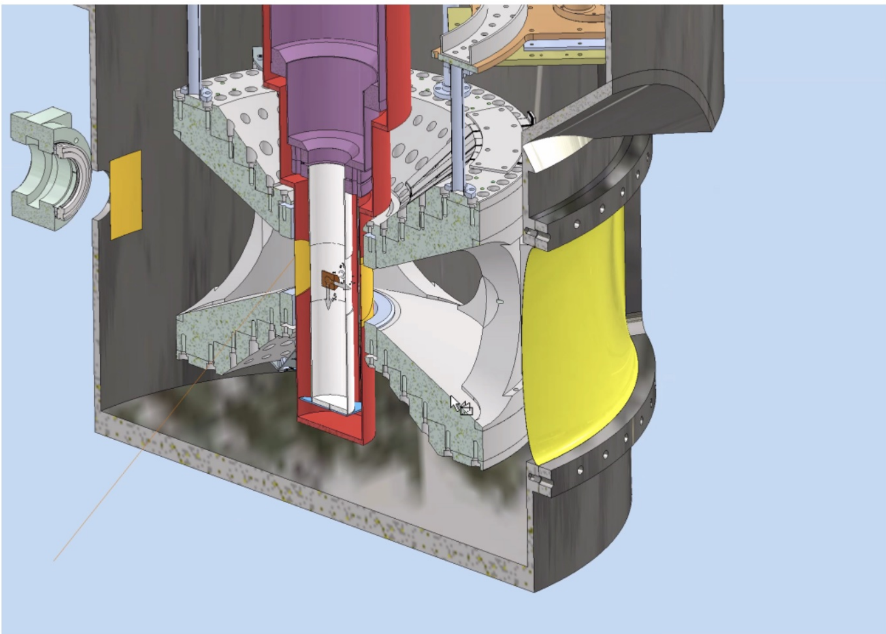

Fig. 27: The entrance and exit windows of the RGH target cryostat.

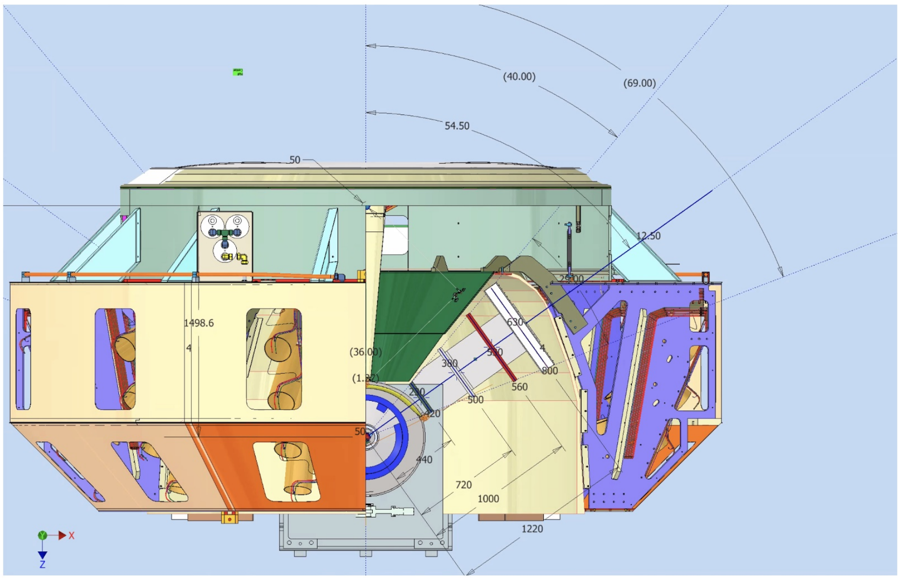

Fig. 28: Top view of the RGH target cryostat and recoil detector showing the clearance and the relevant acceptance angles.

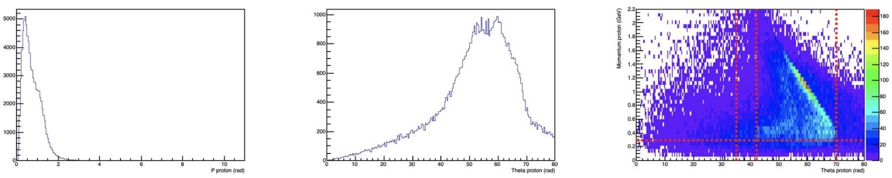

Fig. 29: Momentum and polar angle distributions of the protons from DVCS events.

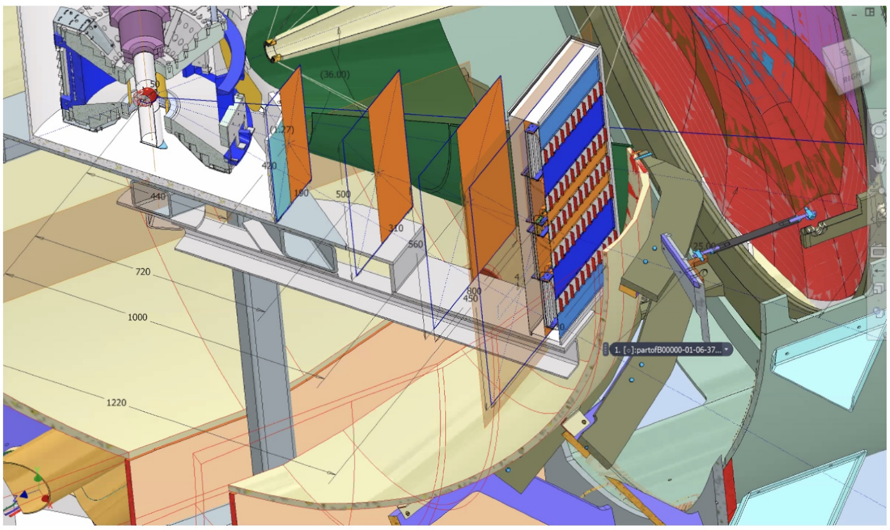

Fig. 30: The support of the RGH recoil detector is a cart able to roll in and out from HTCC and can be realize without interference with HTCC.

4.3.6 Available resources

The RGH detector construction is expected to take 3 years and occurs in parallel to the target development as a main in-kind user contribution. The estimate accounts for the detector realization and commissioning, but assumes no major electronics development is required thanks to the already existing readout systems and the limited amount of readout channels. Groups already involved in the essential technology R&D are part of the RGH recoil project, see Table 3.

Task	Leading Institution	Expertise
μRwell detector	INFN-RM2, INFN-CT	CLAS12 upgrade, ePIC tracking
μRwell readout	INFN-GE, INFN-RM1	SBS GEM tracking readout
TOF detector	DUKE, Orsay	EIC KLM, CLAS12 CND
TOF readout	INFN-GE, INFN-FE	CLAS12 FT and RICH readout
Mechanics	INFN-LNF	CLAS12 RICH mechanics
Integration	JLab	Hall-B infrastructure and beam

Tab. 3: Main elements of the RGH recoil detector with associated leading Institutions.

INFN-RM2 and INFN-CT are working in close contact with the group of Gianni Bencivenni, the inventor of μRwell technology, for the CLAS12 upgrade and the ePIC tracking system. INFN-GE and INFN-RM1 has developed the GEM readout of the SBS experiment. The estimated effort accounts for 6 chambers plus 2 spares, the APV25 readout adaptation to CLAS12 and the possible MPD board upgrade, quantified assuming to connect 15 APV cards to a single MPD as done in SBS, resulting in five new boards plus a spare. Duke is studying a scintillator+SiPM system for the EIC KLM project, Orsay built the CLAS12 CND detector. INFN-GE and INFN-FE has experience in SiPM readout for calorimetry and Cherenkov detectors. The effort estimate accounts for two planes of 300 small scintillating bars instrumented by SiPM, the production of 30 PETIROC front-end boards including 4 spares, and the adaptation of existing electronics to RGH needs. INFN-LNF has been responsible of the CLAS12 RICH mechanics. The mechanics and integration accounts for the installation tools and the required services (power supply and cabling, gas system, slow control, interlock).

The involved groups ensure adequate expertise and workforce to cover both hardware and software needs.

4.4 Luminosity

The CLAS collaboration has completed experimental runs with both liquid hydrogen and deuterium targets, and has reached the design luminosity of $10^{35}\,\mathrm{cm}^{-2}\mathrm{s}^{-1}$ with a deuterium target and 45 nA electron beam current. This is much higher than the nominal luminosity $\mathcal{L} = 5 \times 10^{33}\,\mathrm{cm}^{-2}\mathrm{s}^{-1}$ assumed for the RGH experiments. The ongoing high-lumi project aims to complement the CLAS12 tracking with a front layer of μ-Rwell detectors, able to improve the spatial resolution and rate capability of CLAS12 tracking in the most critical region close to the interaction point, and support a factor two increase in luminosity.

With a dynamically polarized ammonia target, the luminosity is no longer limited by the target polarization lifetime, but by the background induced on the open-acceptance spectrometer. CLAS12 has measured the hit occupancy levels in the Drift Chambers (DC), the most sensitive detectors, as a function of the beam intensity and solenoid current. The typical occupancy is driven by Moeller scatterings in the target and secondary interactions in the shielding around the downstream beam pipe, in the detector structure and in the air filling the experimental hall. CLAS12 simulations reproduce data within an acceptable 30% level.

For the RGH experiments, where the CLAS12 solenoid is replaced by the target 5T transverse polarizing field, the Moeller backgroud is no longer contained inside the beam pipe, but is mainly trapped inside the target region. The baseline of the RGH experiments is to run with no Forward Tagger (FT-OFF) and with additional shielding elements installed to minimize the secondary interactions.

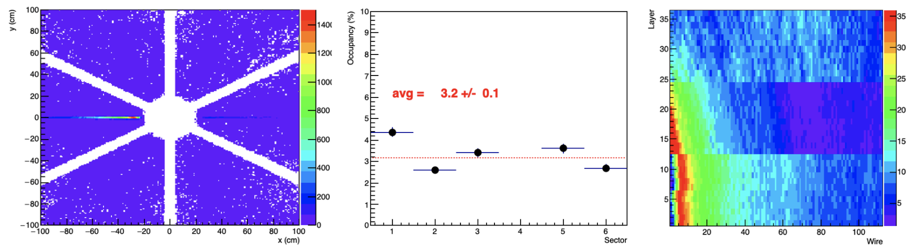

Fig. 31: Simulation results at the nominal RGH luminosity. Background hit distribution on the first DC tracking layer with visible the so-call sheet-of-flame in sector 4 (left). Mean hit occupancy for all DC layers but 4 (center). Hit occupancy per single layer and wire on sector 4 (right).

The RGH background has an additional peculiar component, due to the energy loss of the beam particles passing without interaction through the target. If the loss is big enough, the particle is bent outside the pipe and into the detector acceptance. Such a background is concentrated in the bending plane of the 5T target magnet, creating the so-called *sheet-of-flame*, see Fig. 31 (left). With a vertical magnetic field, the sheet-of-flame will illuminate sector 4 to a level that could be hardly sustainable with the present DC readout, able to record just a single hit in the extended readout gate (between 0.5 μs and 1.5 μs depending on the drift cell size). As a conservative approach, this work assumes

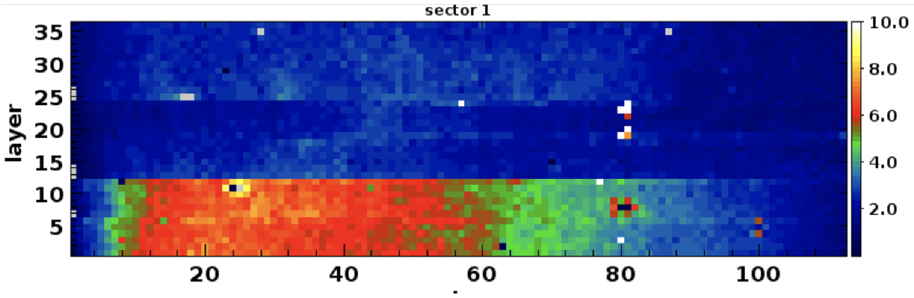

Fig. 32: Typical RGC occupancies as measured by CLAS12 the online monitor during the RGC run with a NH_3 target.

to switch off the critical DC layers in sector 4 (no tracking), and operate the other sectors up to a maximum tolerable occupancy rate of 6-8% as already achieved (even with higher occupancy hot-spots) during the RGC data-taking on longitudinally polarized NH_3 and ND_3 targets , see Fig. 32. This corresponds to the design RGH luminosity of 5×10^{33} cm^{-2}s^{-1}, once a conservative factor 2 is used to account for the different DC readout gates in simulations, see Fig. 31 (center), and real data.

There are concrete possibilities to exceed the conservative luminosity estimate above. RGH will benefit from the ongoing tracking improvements based on machine learning techniques [63, 64]. With the addition of the μ-Rwell tracking layer under development for the CLAS12 high-lumi project, a significant improvement in luminosity is expected (up to a factor two). Optimization studies are ongoing to adapt the CLAS12 background shielding to RGH. Possible mitigation measures can be introduced to partially operate the critical DC layers in sector 4. These includes switching off just the DC wires close to the beam where the background particles concentrate and compensate with the high-lumi tracking layer, see Fig. 31 (right), veto the events with multiple particles as resolved by the high-lumi tracking layer, upgrade the DC readout to process multiple hits in the readout gate. An interesting option is to rotate the target by 90 degrees in order to align the sheet-of-flame with the torus coil shadow. All these developments are being pursued to maximize the physics output of RGH experiments, with the possibility to overcome what has been projected at the time of the proposal.

5 Kinematics

RGH will run with the torus at nominal current. The solenoid will be off and in parking position. The Central Detector will be substitute by the RGH recoil detector.

5.1 DVCS

In RGH, the recoil proton acceptance is limited in azimuthal angles (to less than ±25 degree) by the target holding magnet structure. However, the RGH recoil has been designed to intercept the most populated interval of polar angles, between 40 and 80 degree. As a consequence, the phase space coverage is similar to the one of RGC, the experiment using a longitudinally polarized target inside the CLAS12 Central Detector and solenoid, see Figure 33. Figure 34 shows instead the kinematic coverage, in the RGH setup including proton recoil detector, for the relevant proton-DVCS variables.

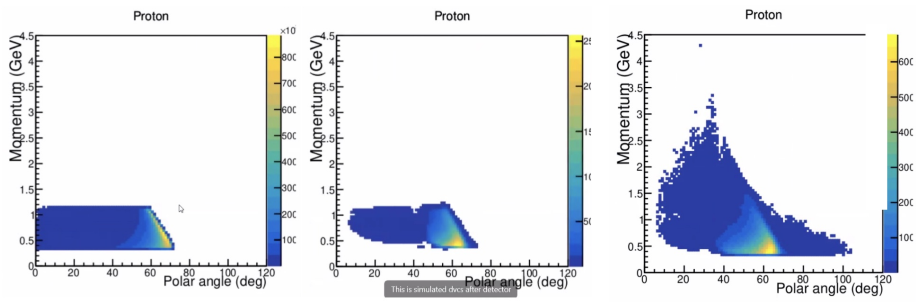

Fig. 33: Proton kinematics in DVCS reaction at 10.6 GeV beam momentum. Generated protons (left), protons inside the RGH acceptance (center), and protons detected in CLAS12 during the RGA run (right).

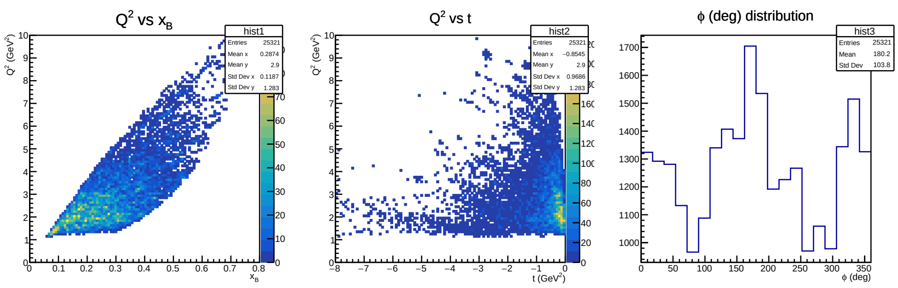

Fig. 34: From left to right: Q^2 vs x_B, Q^2 vs t, and ϕ distributions for proton DVCS events simulated in RGH conditions.

5.2 SIDIS

The support structure of the RGH target magnet is designed to essentially preserve the forward acceptance and, thus, the SIDIS phase space, see Figure 35. The missing sector (sector 4) does not limit the phase space due to the rotational symmetry of the reaction mechanism, which is defined with respect to the lepton scattering plane. A multi-dimensional binning is possible, covering an extended range in x and Q^2, see Figure 36. In all the (x, Q^2) bins, there is coverage in the relevant values of the hadron fractional energy z (from 0.2 to 0.8) and transverse momentum $P_\perp$ (up to 1 GeV/c), see Figures from 37 to 40.

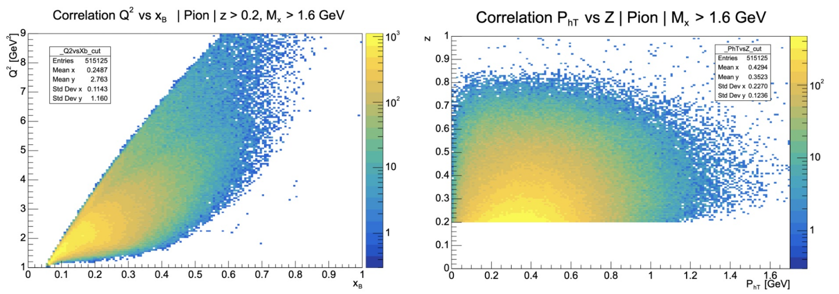

Fig. 35: Proton kinematics in DVCS reaction at 10.6 GeV beam momentum. Generated protons (left), protons inside the RGH acceptance (center), and protons detected in CLAS12 during the RGC run (right).

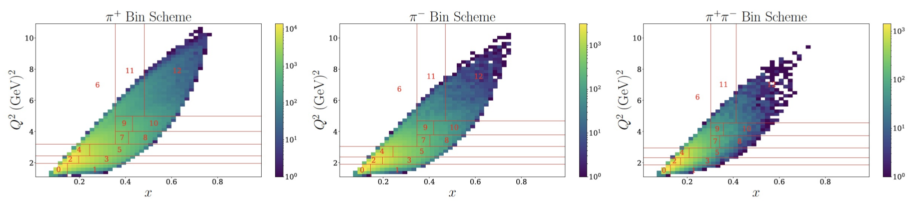

Fig. 36: Possible bin scheme in x and Q^2 for SIDIS events with a leadaing positive pion (Left), negative pion (center) and pion pair (right).

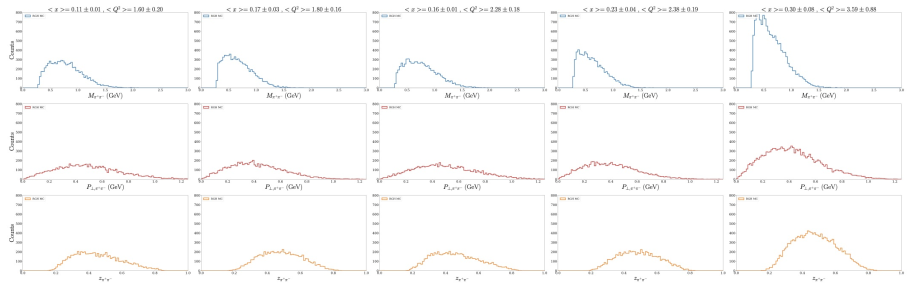

Fig. 37: Distribution of transverse momentum (top row) and fractional energy z (botton row) of SIDIS pion pair is various (x, Q^2) bins.

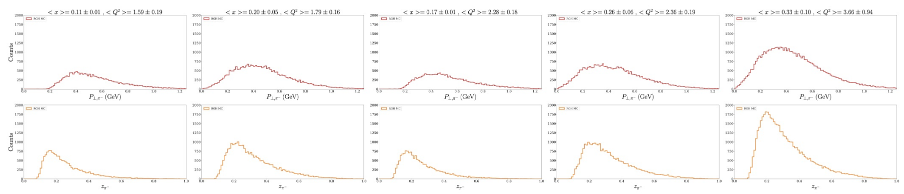

Fig. 38: Distribution of transverse momentum (top row) and fractional energy z (botton row) of SIDIS negative pions is various (x, Q^2) bins.

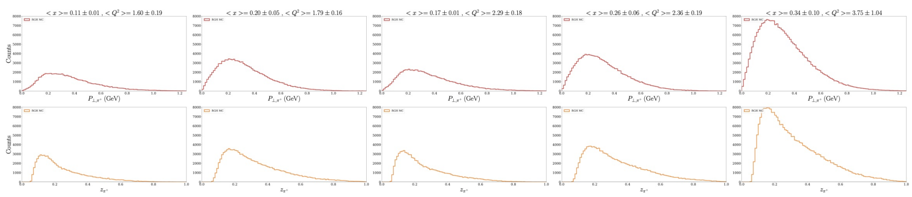

Fig. 39: Distribution of transverse momentum (top row) and fractional energy z (botton row) of SIDIS positive pions is various (x, Q^2) bins.

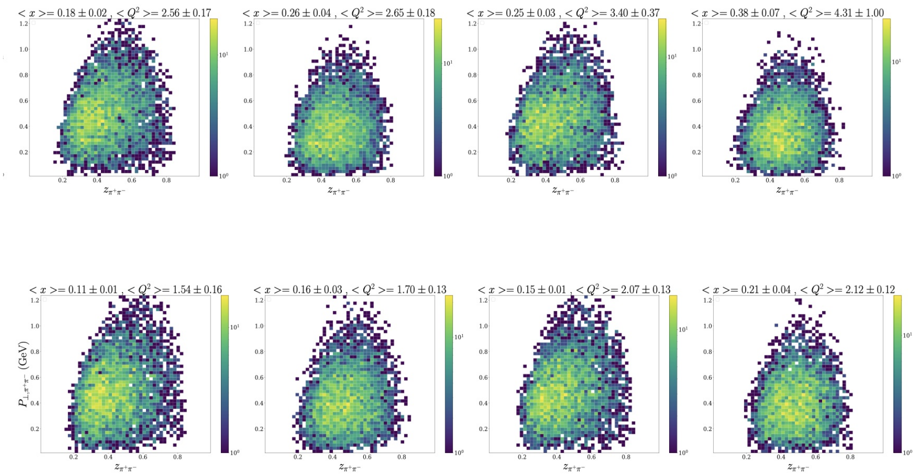

Fig. 40: Correlation between transverse momentum and fractional energy z of SIDIS positive pions is various (x, Q^2) bins.

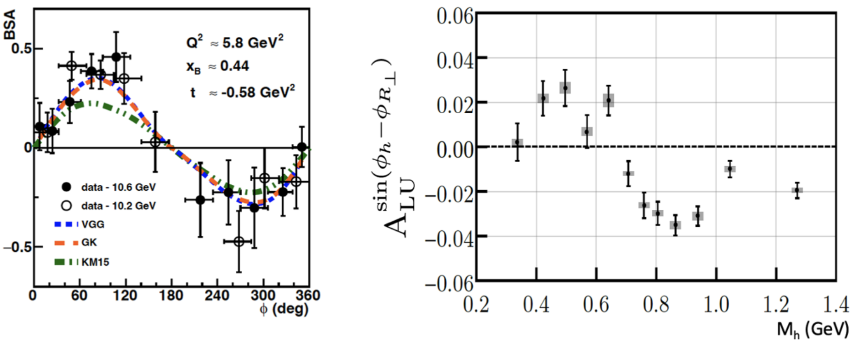

Fig. 41: Examples of CLAS12 published results on beam-spin asymmetry observables based on just a fraction of the recorded statistics. Left: DVCS asymmetry as a function of the azimuthal angle ϕ compared to phenomenological models [65]. Right: SIDIS dihadron asymmetry found to be not-zero for the first time [66].

6 Projections

The RGH projections are based on solid grounds, as they refer to a running experiment and a consolidated target technology. The luminosity is not defined by any target irreducible limits, but by the capability in containing the background level in the experiment, something that is manageable and for which there are many concrete prospects of improvement.

Physics analyses are in progress based on the 10.6 GeV data. CLAS12 results for both the SIDIS and exclusive channels have been published by the Collaboration and presented at conferences. As examples, published beam-spin asymmetries of DVCS events, dihadron and π^+ SIDIS events, based on a fraction of the recorder statistics, are shown in Fig. 41 and Fig. 42 (left), respectively. Data confirm that CLAS12 allows for a much extended reach inside the DIS regime (large Q^2) with respect to CLAS and the valence region (large x) with respect to previous experiments, with an unprecedented statistical precision. With the improved knowledge of the instrumental effects, and the refinement of the calibration procedures and reconstruction algorithms, further progresses are expected towards the best CLAS12 performance before the start of RGH experiments.

6.1 Semi-inclusive Physics

Due to the definition of an orthogonal direction, transverse single-spin asymmetries (TTSAs) are key observables for the access of transverse momentum dependent parton distribution functions (TMDs) [69]. The extraction of TMDs is a focus of the nuclear physics community to access the 3D momentum structure of the proton.

Exemplary different global extractions of transversity are shown in Fig. 42 (right). The precision of the extractions and their compatibility becomes worse

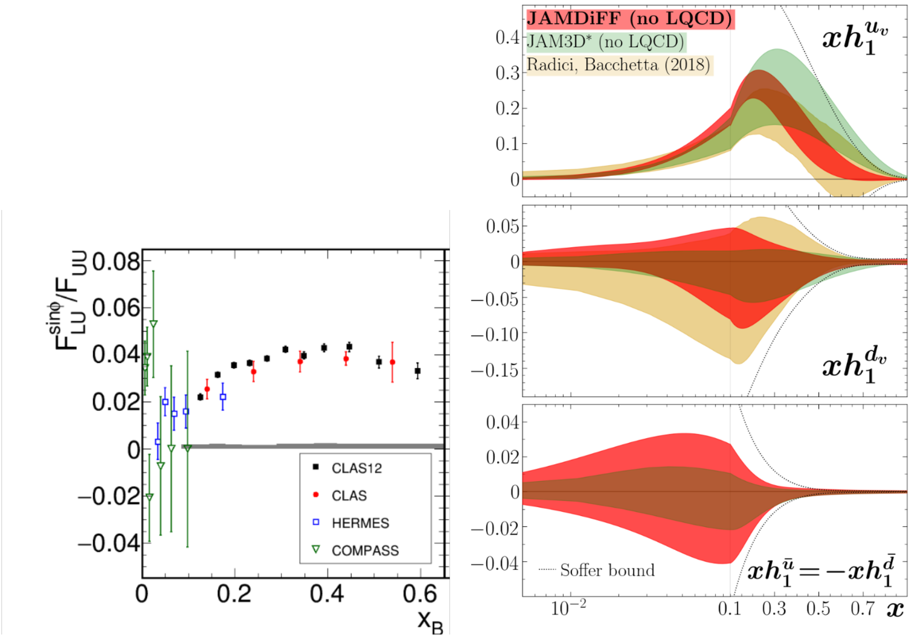

Fig. 42: Left: Beam-spin asymmetries measured by CLAS12 as a function of Bjorken x compared with world data. Figure from [67]. Right: Current extractions of transversity from SIDIS, pp and e^+e^- data. Figure from [68]. Legacy data is mainly limited to $x < 0.3$. This lack of data in the valence region explains the larger uncertainty and difference between the transversity extractions.

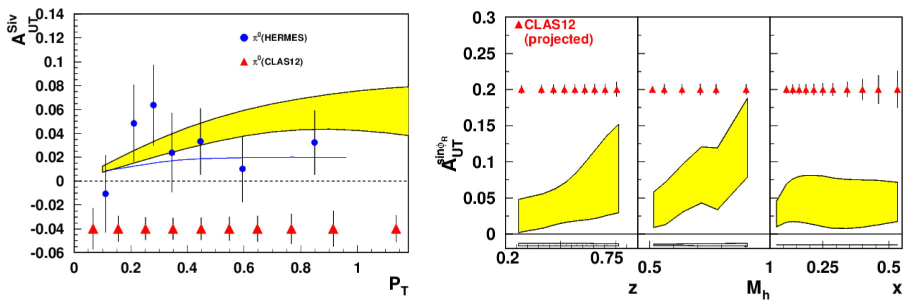

Fig. 43: Left: Projection for the Sivers SSA versus P_T, for a given bin in x and z. The yellow band shows the calculation from JAM3D-22 [12] with relative uncertainty band, and the blue line shows calculations of Pavia group in the kinematical point $x = 0.3$, $Q^2 = 3$ GeV, and $z = 0.4$. HERMES points are the only existing TTSA measurement for SIDIS π^0 up to now [26]. Right: Projected dihadron TTSA as a function of relevant kinematical variables: z, M_h, and x. The yellow band shows the variation of theoretical predictions of the asymmetry due to unknown polarized dihadron fragmentation funcions (DiFFs). Red points show the projected statistical error bars for RGH.

in the valence-quark region. This is due to the lack of data for $x > \approx 0.3$. Since the magnitude of transversity is peaking in the same region, this leads to significant uncertainties on the tensor charge, the integral of the transversity function over x. The tensor charge can be compared with lattice calculations and is also needed to calculate Beyond Standard-Model phenomena in certain scenarios of new physics with tensor coupling or particle electric dipole moment. World data for the longitudinal beam-spin asymmetries (BSAs) compared with CLAS12 extraction from RGA are shown in Fig. 42 (left). We expect a similar x coverage for RGH reaching up to $x \approx 0.6$. This would cover e.g. the whole peak structure in current transversity extractions.

Other TMDs like the Sivers function are also likely dominated by the valence region, thus a similar argument for the importance of the CLAS12 TTSAs holds. Recent measurements of BSAs indicate possible strong contributions to inclusive pion spin asymmetries from vector meson (VM) decays. In addition, several JLab proposals have been approved to study longitudinal photon contributions in inclusive pion multiplicities. The Sivers effects receives also a contribution from longitudinal photons, which was never measured or quantified, suggesting that the systematics of the Sivers effect measurements may be currently underestimated. This makes the measurements of all observables in semi-inclusive π^0 production, and the Sivers effect in particular, critical: The neutral pion is known to receive a minor contribution from exclusive VM decays, and even in exclusive limit, minor contributions from longitudinal photons. The high statistics of CLAS12 at large x, where the effects are significant, would allow detailed measurements of TTSAs, in particular as a function of the transverse momentum of hadrons. Understanding the transverse momentum dependences of all kind of observables in polarized SIDIS, including multiplicities and the Sivers asymmetry, has been always a challenging task for theory, but is instrumental in providing important information for the phenomenological studies, and a validation of the underlying dynamics description. The contributions from VM, and the strong correlations between hadrons produced in SIDIS, make the measurements with dihadrons critical for the interpretation of complex observables, such as single-spin asymmetries, and transverse single spin asymmetries, in particular. A significant Sivers effects was recently predicted for dihadrons [70].

Data-driven projections for SIDIS observables have been derived following the method explained in Section 6.2, and benefit from the fact that the forward acceptance of pions, and π^0 in particular, is largely preserved. Note that in the SIDIS case, where nuclear interactions (on Nitrogen) cannot be kinematically suppressed, the target dilution factor $f = 3/17$ should be treated as polarization and multiply the error instead of the yield.

One example for the projected Sivers asymmetry measurement with CLAS12 as a function of the transverse momentum of neutral pions in a small bin in x is shown in Fig. 43 (left). The projection for a particular transverse single spin asymmetry for dihadrons, providing access to transversity measurements, is shown in Fig. 43 (right).

The RGH pseudo-data have been used to estimate the impact on our present knowledge of the flavor-separated tensor charge. RGH data will significantly reduce the present uncertainty of the di-hadron asymmetry, see Figure 44. As a consequence, the experimental input to the phenomenological fits becomes competitive with that of the lattice, offering for the first time an effective benchmark [71], see Figure 45. Currently, inputs from lattice dominate the common phenomenological fits and no conclusion on the apparent tension with experiments can be drawn. With RGH data the discrepancy could be solved, or become manifest.

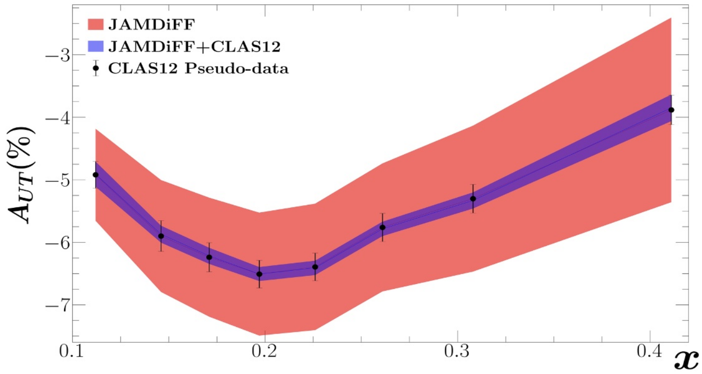

Fig. 44: Impact of the RGH pseudo-data on the JAMDiFF phenomenological fit, from [71].

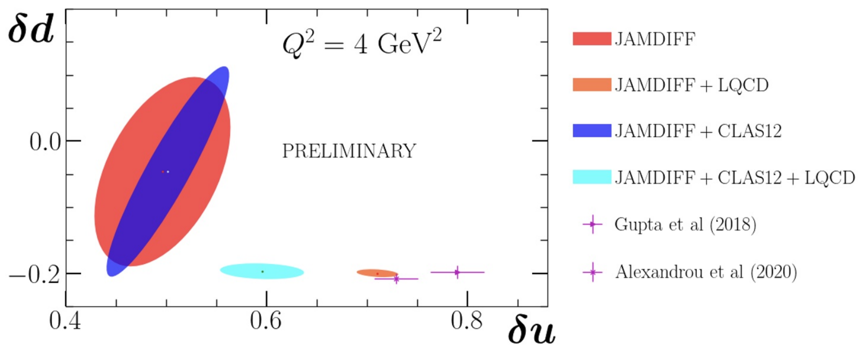

Fig. 45: Impact of the RGH pseudo-data on the tensor charge δu of the u quark flavor, from [71]. RGH data-set will be competitive with lattice calculations and provide an effective benchmark.

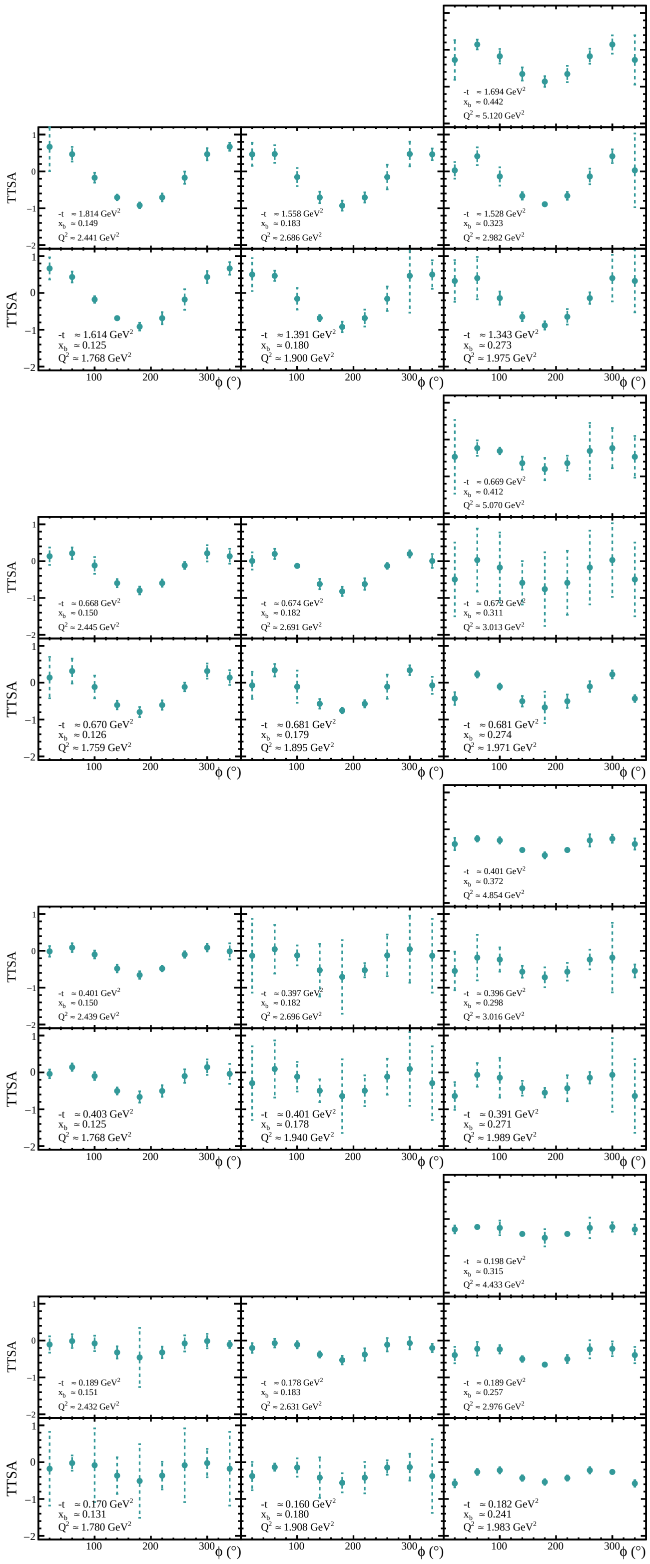

Fig. 46: Projections for the transverse target spin asymmetry versus ϕ which will be obtained by RGH for the proton-DVCS reaction, for 4 bins in $-t$ (each block of 7 plots, from top to bottom), for 3 bins in x_B (along the horizonthal axis of each block of plots), and 3 bins in Q^2 (along the vertical axis of each block of plots). The average kinematics is indicated on each plot.

6.2 DVCS

Measuring DVCS on a transversely polarized proton target is crucial as the transverse-target spin asymmetry (TTSA) is the DVCS observable having the strongest sensitivity to the GPD E of the proton. Knowing E is paramount in order to extract the quarks' angular momentum contribution to the proton spin via the Ji sum rule [18].

Projections for the DVCS TTSA that will be obtained by RGH have been computed using a data-driven method to estimate the yields. Proton-DVCS yields (Y) were extracted using data from the RGA Fall 2018 period. Acceptances were computed for both the RGH and the RGA configurations using the CLAS12 GEANT4-based simulation software, gemc, and the CLAS12 reconstruction. The RGA yields were multiplied, for each kinematic bin in $(Q^2, x_B, -t, \phi)$, by the ratio of the RGH and RGA acceptance for pDVCS. This product was then multiplied by the ratio of the integrated luminosities of RGH and RGA. This is summarized in Eq. 1:

$$Y_{RGH}(i) = Y_{RGA}(i) \cdot \frac{Acc_{RGH}(i)}{Acc_{RGA}(i)} \cdot \frac{L_{RGH}}{L_{RGA}} \cdot \frac{3}{17}, \quad (1)$$

where i labels the 4-dimensional bin in $Q^2, x_B, -t, \phi$, $L_{RGH} = 100$ days $\cdot\, 5 \cdot 10^{33}$ cm^{-2}s^{-1}, $L_{RGA} = 16$ days $\cdot\, 0.8 \cdot 10^{35}$ cm^{-2}s^{-1}, and the factor 3/17 accounts for the fraction of protons from hydrogen in NH_3.

The grid of 4-dimensional bins was established according to the statistics obtained with Eq. 1. The TTSA was computed, as a function of ϕ, at the average kinematics of each $(Q^2, x_B, -t)$ using the VGG model. The obtained yields for RGH were used to deduce statistical error bars for the TTSA, according to the formula:

$$\sigma_A(i) = \frac{1}{P} \cdot \sqrt{\frac{1 - (P \cdot A)^2}{Y_{RGH}(i)}}, \quad (2)$$

where A is the value of the TTSA, and P is the target polarization, assumed to be 85%. Note that the selection of the exclusive kinematics largely suppress the nuclear interactions (on Nitrogen) and therefore the target dilution $f = 3/17$ reduces the yield, but does not suppress the asymmetry as in the case of SIDIS.

In order to test the sensitivity of the projected data to the GPD E, various sets of quark's angular momenta J_u and J_d were used to compute the TTSA with the VGG model. In this model, indeed, J_u and J_d enter directly the parameterization of the GPD E, and they can be chosen as input parameters.

The projections for the TTSA are shown in Fig. 46, plotted as a function of ϕ for each bin in $(Q^2, x_B, -t)$ for the case $J_u = -0.5$, $J_d = -0.1$. Figure 47 shows the transverse-target spin asymmetry versus ϕ for one of the $(Q^2, x_B, -t)$ bins shown in Fig 46, and for three sets of values of J_u and J_d (brown: $J_u = 0.5$, $J_d = 0.1$; cyan: $J_u = -0.5$, $J_d = -0.1$; blue: $J_u = 0.2$, $J_d = 0$). The size of the projected error bars allows us to distinguish between the three hypotheses. For comparison, the asymmetry as computed with the PARTONS code is also shown (in black).

This is even more evident in Fig. 48, which shows the moments A_{UT}, extracted by fitting the TTSA with the function $A_{UT} \sin(\phi - \phi_S) \cos\phi$. The colors indicate the three sets of values given to VGG for J_u and J_d. Aside from some

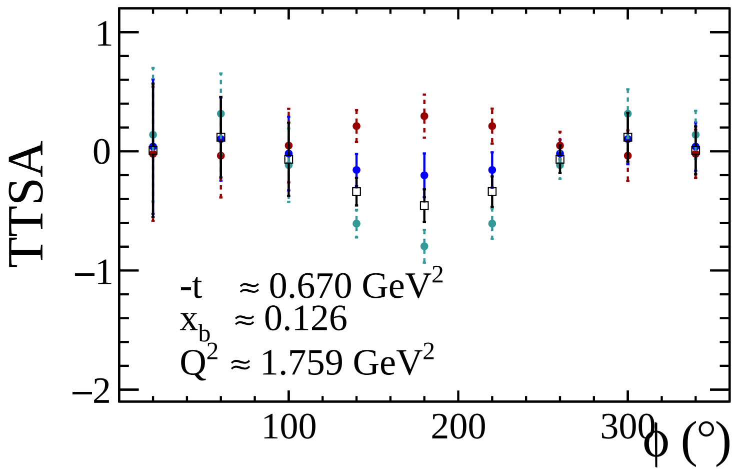

Fig. 47: Projections for the transverse target spin asymmetry versus ϕ which will be obtained by RGH for the proton-DVCS reaction, for one $(Q^2, x_B, -t)$ bin, and for 3 sets of values of the quark's angular momenta J_u and J_d, as computed by the VGG model. Brown: $J_u = 0.5$, $J_d = 0.1$; cyan: $J_u = -0.5$, $J_d = -0.1$; blue: $J_u = 0.2$, $J_d = 0$. For comparison, in black are shown the values computed with PARTONS. The error bars reflect the expected statistics of RGH.

kinematic corner were the expected statistical precision will be poorer, such as at low x_B and $-t$ in the second Q^2 bin, the precision of the data will be enough to discriminate between the various model hypotheses. The only existing published data for this observable, measured by HERMES [33], are included in Fig. 48, and represented by the 4 black points in the bottom-left plot. The RGH experiment will not only improve on the statistical precision of that particular kinematics, but will also extend the measurement of the TTSA over a vast phase space region. The inclusion of the RGH pDVCS data to global fits for the extraction of GPDs will strongly constrain the poorly known GPD E of the proton. This will allow us, in particular, to map the t-dependence of the imaginary part of the GPD E, and thus to make an important step toward the extraction of the quarks' angular momentum contribution to the proton spin via the Ji sum rule.

6.3 Systematic uncertainty

Note that RGH presently assumes to run at a luminosity that is 20 times lower than the nominal CLAS12 value. As a consequence, the precision of RGH results is expected to be statistically dominated.

At JLab, there is a consolidated knowledge of the NH3 target polarization, which will only increase with the recent CLAS12 RGC run. When using NMR to measure the NH_3 target polarization, the typical uncertainty is 4-5%. The SANE experiment in Hall C (similar target geometry) quotes an uncertainty in the dilution factor of 2% [48].

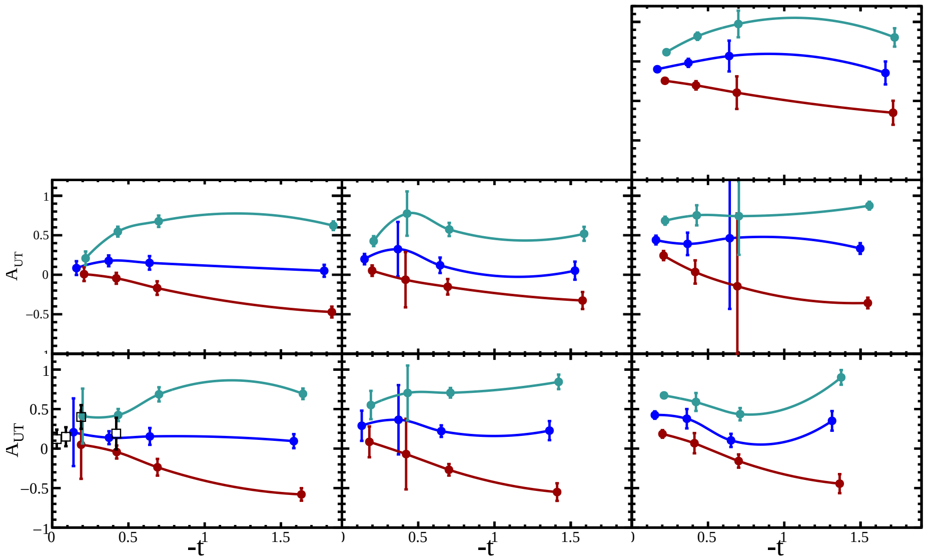

Fig. 48: Projections for the A_{UT} moments which will be obtained by RGH for the proton-DVCS reaction, for the full grid of $(Q^2, x_B, -t)$ bins, and for 3 sets of values of the quark's angular momenta J_u and J_d, as computed by the VGG model. The error bars reflect the expected statistics of RGH. The color code is the same as in the caption of Fig. 47. The 4 black points in the bottom-left plot are the HERMES data [33].

CLAS12 published analyses of SIDIS and DVCS observables present systematic uncertainties of acceptance and radiative corrections that are good references for RGH. Possible effects of the missing sector will be mitigated by the microwave-induced swap of the target polarization and are expected to not significantly increase the acceptance uncertainty because CLAS12 acceptance is anyway azimuthally not uniform. The RGH recoil is based on technologies (MGPD tracking and scintillating materials) that are already in use at CLAS12. The effect of the recoil detector performance was studied varying resolution and kinematic range, and typical variations were found to be within 5%. Particle identification, accidental coincidences, and the photoproduction of electrons that are misidentified as the scattered electron are typically found to be negligible. The main contributions to the systematic uncertainty are listed for the different reactions of interest from Table 4 to Table 6.

Source	Systematic Uncertainty
Target polarization	5 %
Target dilution	2 %
Radiative effects	3 %
Acceptance and bin-migration	3 %

Tab. 4: Estimated main contributions to the systematic uncertainty for SIDIS single hadron.

Source	Systematic Uncertainty
Target polarization	5 %
Target dilution	2 %
Baryonic contribution from target fragmentation	1-6%
Bin migration close to ρ mass	1-10%

Tab. 5: Estimated main contributions to the systematic uncertainty for SIDIS di-hadron.

Source	Systematic Uncertainty
Target polarization	5 %
Target dilution	1 %
Recoil acceptance	5 %

Tab. 6: Estimated main contributions to the systematic uncertainty for DVCS.

7 Beam Time Request

The required days of data-taking for the RGH physics and calibration runs are listed in Table 7. The days are calculated assuming the accelerator is avaliable at all times with an 100% duty cycle.

Target operations account for annealing and sample exchange. Assuming 1 nA impinging on a (1.5 dia x 2) cm^3 ammonia target, each ammonia sample will last for 4-5 days of beam before annealing is necessary. The samples will be annealed in place as already done in the past. With two interchangeable cells in the ladder and some days of background running, one would only need to anneal every two weeks and replace the samples after about two months. TE calibrations of the NMR should be performed prior to annealing, so the entire process will take about 12 hours.

Beam Energy (GeV)	Beam Current (nA)	Beam Requirements	Target	Material Thickness (mg/cm^2)	Beamtime (days)
10.6	1	Polarized	NH_3	1040	100
10.6	1	Polarized	$^{12}C, CH_2$	1040, 1040	8
10.6	1	Polarized	Empty	na	2
			Operations		10
Total					120

Tab. 7: Data-taking time required to achieve the proposed physics goals assuming the accelerator is available at all times (100% duty cicle)

8 Summary

The RGH experiments at CLAS12 offer a compelling physics program that has the potential to provide unprecedented information on the peculiar parton dynamics within the nucleon and during fragmentation. It will complement the information gathered with unpolarized and longitudinally polarized targets by the same experiment. Since the approval in 2012, the interest in this field of research has grown worldwide and culminated with the start of the EIC Project. The theoretical understanding and lattice calculations have made important progresses, which consolidate the interest in new experimental results. At the same time, a comprehensive program has been pursued at JLab to understand and overcome the technical challenges connected with running a transversely polarized target inside CLAS12. The adopted solution is based on extended validation tests of target alternatives with electron beam, real-data and concrete experience acquired so far running the experiment, choice of consolidated technologies to favor physics over development. CLAS12 has been already complemented with the additional particle-identification detector anticipated in the proposal (RICH), and further upgrades are planned that will boost the RGH reach. We request the PAC to allow the conclusion of this effort and approve the requested beam time (120 days).

References

[1] JLab PAC Report. *https://www.jlab.org/exp_prog/PACpage/PAC39/PAC39%20Final_Report.pdf*, 2012.

[2] JLab PAC High-Impact Selection. *https://www.jlab.org/exp_prog/PACpage/High_Impact_Proposals.pdf*, 2014.

[3] H. Avakian et al. Transverse spin effects in SIDIS at 11 GeV with a transversely polarized target using the CLAS12 Detector. *https://www.jlab.org/exp_prog/proposals/12/C12-11-111.pdf*, 2012.

[4] H. Avakian et al. Measurement of transversity with dihadron production in SIDIS with transversely polarized target. *https://www.jlab.org/exp_prog/proposals/12/PR12-12-009.pdf*, 2012.

[5] H. Avakian et al. Deeply Virtual Compton Scattering at 11 GeV with transversely polarized target using the CLAS12 Detector. *https://www.jlab.org/exp_prog/proposals/12/PR12-12-010_rv.pdf*, 2012.

[6] JLab PAC Report. *https://www.jlab.org/sites/default/files/PAC/PAC52/PAC52%20REPORT%202024.pdf*, 2024.

[7] A. Accardi et al. Electron Ion Collider: The Next QCD Frontier: Understanding the glue that binds us all. *Eur. Phys. J. A*, 52(9):268, 2016.

[8] R. Abdul Khalek et al. Science Requirements and Detector Concepts for the Electron-Ion Collider: EIC Yellow Report. *Nucl. Phys. A*, 1026:122447, 2022.

[9] H. Avakian, A. Bressan, and M. Contalbrigo. Experimental results on TMDs. *Eur. Phys. J. A*, 52(6):150, 2016. [Erratum: Eur.Phys.J.A 52, 165 (2016)].

[10] M. Pitschmann, C.-Y. Seng, C.D. Roberts, and S.M. Schmidt. Nucleon tensor charges and electric dipole moments. *Phys. Rev. D*, 91:074004, 2015.

[11] A. Courtoy, S. Baeßler, M. González-Alonso, and S. Liuti. Beyond-Standard-Model Tensor Interaction and Hadron Phenomenology. *Phys. Rev. Lett.*, 115:162001, 2015.

[12] L. Gamberg, M. Malda, J.A. Miller, D. Pitonyak, A. Prokudin, and N. Sato. Updated QCD global analysis of single transverse-spin asymmetries: Extracting H˜, and the role of the Soffer bound and lattice QCD. *Phys. Rev. D*, 106(3):034014, 2022.

[13] C. Alexandrou. Recent progress on the study of nucleon structure from lattice QCD and future perspectives. *SciPost Phys. Proc.*, 3:015, 2020.

[14] A. Bacchetta, D. Boer, M. Diehl, and P.J. Mulders. Matches and mismatches in the descriptions of semi-inclusive processes at low and high transverse momentum. *JHEP*, 08:023, 2008.

[15] M. Radici and A. Bacchetta. First Extraction of Transversity from a Global Analysis of Electron-Proton and Proton-Proton Data. *Phys. Rev. Lett.*, 120(19):192001, 2018.

[16] I. Garzia and F. Giordano. Transverse-momentum-dependent fragmentation functions in e^+e^- annihilation. *Eur. Phys. J. A*, 52(6):152, 2016.

[17] M.J. Skoby. High Precision Measurement of Transversity Using Di-hadron Correlations in $p\hat{}^{+p}$ Collisions at $\sqrt{s_{NN}} = 500$ GeV. *Int. J. Mod. Phys. Conf. Ser.*, 40:1660038, 2016.

[18] X.-D. Ji. Gauge-Invariant Decomposition of Nucleon Spin. *Phys. Rev. Lett.*, 78:610–613, 1997.

[19] L. Adhikari and M. Burkardt. Angular Momentum Distribution in the Transverse Plane. *Phys. Rev. D*, 94(11):114021, 2016.

[20] N. d'Hose, S. Niccolai, and A. Rostomyan. Experimental overview of Deeply Virtual Compton Scattering. *Eur. Phys. J. A*, 52(6):151, 2016.

[21] A. Bacchetta, M. Diehl, K. Goeke, A. Metz, P.J. Mulders, and M. Schlegel. Semi-inclusive deep inelastic scattering at small transverse momentum. *JHEP*, 02:093, 2007.

[22] S.V. Goloskokov and P. Kroll. Transversity in hard exclusive electroproduction of pseudoscalar mesons. *Eur. Phys. J. A*, 47:112, 2011.

[23] S.V. Goloskokov and P. Kroll. An Attempt to understand exclusive pi+ electroproduction. *Eur. Phys. J. C*, 65:137–151, 2010.

[24] G.D. Alexeev et al. Transverse-spin-dependent azimuthal asymmetries of pion and kaon pairs produced in muon-proton and muon-deuteron semi-inclusive deep inelastic scattering. *Phys. Lett. B*, 845:138155, 2023.

[25] G.D. Alexeev et al. High-Statistics Measurement of Collins and Sivers Asymmetries for Transversely Polarized Deuterons. *Phys. Rev. Lett.*, 133(10):101903, 2024.

[26] A. Airapetian et al. Azimuthal single- and double-spin asymmetries in semi-inclusive deep-inelastic lepton scattering by transversely polarized protons. *JHEP*, 12:010, 2020.

[27] M.G. Alexeev et al. Measurement of P_T-weighted Sivers asymmetries in leptoproduction of hadrons. *Nucl. Phys. B*, 940:34–53, 2019.

[28] G.D. Alexeev et al. Final COMPASS Results on the Transverse-Spin-Dependent Azimuthal Asymmetries in the Pion-Induced Drell-Yan Process. *Phys. Rev. Lett.*, 133(7):071902, 2024.

[29] C. Cocuzza, A. Metz, D. Pitonyak, A. Prokudin, N. Sato, and R. Seidl. Transversity Distributions and Tensor Charges of the Nucleon: Extraction from Dihadron Production and Their Universal Nature. *Phys. Rev. Lett.*, 132(9):091901, 2024.

[30] M. Boglione, U. D'Alesio, C. Flore, J.O. Gonzalez-Hernandez, F. Murgia, and A. Prokudin. Simultaneous reweighting of Transverse Momentum Dependent distributions. *Phys. Lett. B*, 854:138712, 2024.

[31] H. Gao et al. Target Single Spin Asymmetry in Semi-Inclusive Deep-Inelastic $(e, e'^{\pm})$ Reaction on a Transversely Polarized ^{3}He Target at 8.8 and 11 GeV - E12-10-006. *https://www.jlab.org/exp_prog/proposals/10/PR12-10-006.pdf*, 2010.

[32] H. Gao et al. Target Single Spin Asymmetry in Semi-Inclusive Deep-Inelastic $(e, e'^{\pm})$ Reaction on a Transversely Polarized Proton Target - E12-11-108. *https://www.jlab.orgexp_progproposals11PR12-11-108.pdf*, 2011.

[33] A. Airapetian et al. Measurement of Azimuthal Asymmetries With Respect To Both Beam Charge and Transverse Target Polarization in Exclusive Electroproduction of Real Photons. *JHEP*, 06:066, 2008.

[34] A. Airapetian et al. Measurement of double-spin asymmetries associated with deeply virtual Compton scattering on a transversely polarized hydrogen target. *Phys. Lett. B*, 704:15–23, 2011.

[35] O. Bessidskaia Bylund, M. Defurne, and P.A.M. Guichon. Recoil proton polarization: A new discriminative observable for deeply virtual Compton scattering. *Phys. Rev. D*, 107(1):014020, 2023.

[36] M. Defurne et al. Recoil Nucleon Polarization in Deeply Virtual Compton Scattering and Neutral Pion Electroproduction in Hall-C - LOI12-23-014. *https:www.jlab.orgexp_progproposals23LOI12-23-014.pdf*, 2023.

[37] M. Čuić, K. Kumerički, and A. Schäfer. Separation of Quark Flavors Using Deeply Virtual Compton Scattering Data. *Phys. Rev. Lett.*, 125(23):232005, 2020.

[38] F. Georges et al. Deeply Virtual Compton Scattering Cross Section at High Bjorken xB. *Phys. Rev. Lett.*, 128(25):252002, 2022.

[39] C. Alexandrou et al. Moments of the nucleon transverse quark spin densities using lattice QCD. *Phys. Rev. D*, 107(5):054504, 2023.

[40] A. Scapellato, C. Alexandrou, K. Cichy, M. Constantinou, K. Hadjiyiannakou, K. Jansen, and F. Steffens. Proton generalized parton distributions from lattice QCD. *Rev. Mex. Fis. Suppl.*, 3(3):0308104, 2022.

[41] P.A. Adderley et al. The Continuous Electron Beam Accelerator Facility at 12 GeV. *Phys. Rev. Accel. Beams*, 27(8):084802, 2024.

[42] V.D. Burkert et al. The CLAS12 Spectrometer at Jefferson Laboratory. *Nucl. Instrum. Meth. A*, 959:163419, 2020.

[43] B. Raydo, S. Boyarinov, A. Celentano, C. Cuevas, R. de Vita, V. Kubarovsky, B. Moffit, S. Niccolai, R. Paremuzyan, and C. Smith. The CLAS12 Trigger System. *Nucl. Instrum. Meth. A*, 960:163529, 2020.

[44] D.S. Carman et al. The CLAS12 Forward Time-of-Flight system. *Nucl. Instrum. Meth. A*, 960:163629, 2020.

[45] M. Contalbrigo et al. The CLAS12 Ring Imaging Cherenkov detector. *Nucl. Instrum. Meth. A*, 964:163791, 2020.

[46] J. Pierce, J. Maxwell, and C. Keith. Dynamically polarized target for the g_2^p and G_E^p experiments at Jefferson Lab. *Nucl. Instrum. Meth. A*, 738:54–60, 2014.

[47] Christopher Keith. A Dynamically Polarized Solid Target for CLAS12. *PoS*, PSTP2017:008, 2018.

[48] J. D. Maxwell et al. Design and Performance of the Spin Asymmetries of the Nucleon Experiment. *Nucl. Instrum. Meth. A*, 885:145–159, 2018.

[49] C. D. Keith, J. Brock, C. Carlin, T. Kageya, V. Lagerquist, J. Maxwell, and P. Pandey. First Use of a Longitudinally Polarized Target with CLAS12. *PoS*, PSTP2022:009, 2023.

[50] Christopher Keith. Design Considerations for a Transversely Polarized Solid Target in Hall B at Jefferson Lab. *PoS*, SPIN2023:214, 2024.

[51] M. Böhm, A. Lehmann, S. Motz, and F. Uhlig. Fast SiPM Readout of the PANDA TOF Detector. *JINST*, 11(05):C05018, 2016.

[52] T. Rostomyan et al. Timing detectors with SiPM read-out for the MUSE experiment at PSI. *Nucl. Instrum. Meth. A*, 986:164801, 2021.

[53] F. Sauli. GEM: A new concept for electron amplification in gas detectors. *Nucl. Instrum. Meth. A*, 386:531–534, 1997.

[54] L. Periale, V. Peskov, P. Carlson, T. Francke, P. Pavlopoulos, P. Picchi, and F. Pietropaolo. Detection of the primary scintillation light from dense Ar, Kr and Xe with novel photosensitive gaseous detectors. *Nucl. Instrum. Meth. A*, 478:377–383, 2002.

[55] R. Chechik, A. Breskin, and C. Shalem. Thick GEM-like multipliers: A Simple solution for large area UV-RICH detectors. *Nucl. Instrum. Meth. A*, 553:35–40, 2005.

[56] Y. Giomataris, P. Rebourgeard, J. P. Robert, and Georges Charpak. MICROMEGAS: A High granularity position sensitive gaseous detector for high particle flux environments. *Nucl. Instrum. Meth. A*, 376:29–35, 1996.

[57] G. Bencivenni, R. De Oliveira, G. Morello, and M. Poli Lener. The micro-Resistive WELL detector: a compact spark-protected single amplification-stage MPGD. *JINST*, 10(02):P02008, 2015.

[58] G. Bencivenni, R. De Oliveira, G. Felici, M. Gatta, M. Giovannetti, G. Morello, and M. Poli Lener. The μ-RWELL for high rate application. *JINST*, 15(09):C09034, 2020.

[59] M.J. French et al. Design and results from the APV25, a deep sub-micron CMOS front-end chip for the CMS tracker. *Nucl. Instrum. Meth. A*, 466:359–365, 2001.

[60] F. Dubinin, N. Boyko, A. Konotop, G. Dolganov, and A. Zhurkina. PET Prototype Based on Scintillation Detectors GAGG-SiPM Coupled to 32-Channel Petiroc2A Chip. *Phys. Part. Nucl. Lett.*, 21(4):715–718, 2024.

[61] T. Saleem, S. Ahmad, J.-B. Cizel, C. De La Taille, M. Morenas, V. Nadig, F. Perez, V. Schulz, S. Gundacker, and J. Fleury. Study experimental time resolution limits of recent ASICs at Weeroc with different SiPMs and scintillators. *JINST*, 18(10):P10005, 2023.

[62] R. Kelleher. A MuID and Hadronic Calorimeter for a Second Detector at the EIC - Talk at the 2024 Fall Meeting of the APS Division of Nuclear Physics. *https://meetings.aps.org/Meeting/DNP24/Session/F12.6*, 2012.

[63] P. Thomadakis, A. Angelopoulos, G. Gavalian, and N. Chrisochoides. Using machine learning for particle track identification in the CLAS12 detector. *Comput. Phys. Commun.*, 276:108360, 2022.

[64] P. Thomadakis, A. Angelopoulos, G. Gavalian, and N. Chrisochoides. Denoising drift chambers in CLAS12 using convolutional auto encoders. *Comput. Phys. Commun.*, 271:108201, 2022.

[65] G. Christiaens et al. First CLAS12 Measurement of Deeply Virtual Compton Scattering Beam-Spin Asymmetries in the Extended Valence Region. *Phys. Rev. Lett.*, 130(21):211902, 2023.

[66] T. B. Hayward et al. Observation of Beam Spin Asymmetries in the Process $ep \to e^{'}\pi^{+}\pi^{-}X$ with CLAS12. *Phys. Rev. Lett.*, 126:152501, 2021.

[67] S. Diehl et al. Multidimensional, High Precision Measurements of Beam Single Spin Asymmetries in Semi-inclusive π^{+} Electroproduction off Protons in the Valence Region. *Phys. Rev. Lett.*, 128(6):062005, 2022.

[68] C. Cocuzza, A. Metz, D. Pitonyak, A. Prokudin, N. Sato, and R. Seidl. First simultaneous global QCD analysis of dihadron fragmentation functions and transversity parton distribution functions. *Phys. Rev. D*, 109(3):034024, 2024.

[69] M. Anselmino, A. Mukherjee, and A.1 Vossen. Transverse spin effects in hard semi-inclusive collisions. *Prog. Part. Nucl. Phys.*, 114:103806, 2020.

[70] H.H. Matevosyan, A. Kotzinian, E.-C. Aschenauer, H. Avakian, and A.W. Thomas. Predictions for Sivers single spin asymmetries in one- and two-hadron electroproduction at CLAS12 and EIC. *Phys. Rev. D*, 92(5):054028, 2015.

[71] Y. Sawaya. Phenomenological fits of di-hadron $\mathrm{A_{UT}}$. *poster at POETIC COnference*, 2025.